

AD-A061 420

NAVAL POSTGRADUATE SCHOOL MONTEREY CALIF

F/G 11/6

THE EFFECTS OF MULTIPLE WELD REPAIRS ON THE ALUMINUM-MAGNESIUM --ETC(U)

SEP 78 G R SPEIGHT

UNCLASSIFIED

NL

1 OF 1
ADA
061420

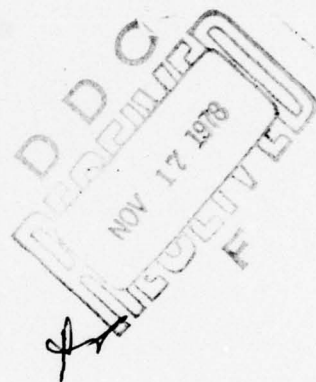
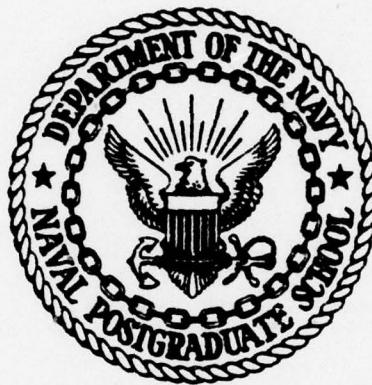
NO
W/0



LEVEL II

P
nu

NAVAL POSTGRADUATE SCHOOL
Monterey, California



DDC FILE COPY
AD A061420

THESIS

6	THE EFFECTS OF MULTIPLE WELD REPAIRS ON THE ALUMINUM-MAGNESIUM ALLOY 5083-O	
11	September 1978	12 94p
by		
10	George R. Speight, Jr.	
Thesis Advisor:		Terry R. McNelley

Approved for Public Release; distribution unlimited

251 450
78 11 13 081

7013

UNCLASSIFIED

SECURITY CLASSIFICATION OF THIS PAGE (When Data Entered)

REPORT DOCUMENTATION PAGE		READ INSTRUCTIONS BEFORE COMPLETING FORM
1. REPORT NUMBER	2. GOVT ACCESSION NO.	3. RECIPIENT'S CATALOG NUMBER
4. TITLE (and Subtitle) THE EFFECTS OF MULTIPLE WELD REPAIRS ON THE ALUMINUM-MAGNESIUM ALLOY 5083-0		5. TYPE OF REPORT & PERIOD COVERED Master's Thesis Sept. 78
7. AUTHOR(s) George R. Speight, Jr.		6. PERFORMING ORG. REPORT NUMBER
9. PERFORMING ORGANIZATION NAME AND ADDRESS Naval Postgraduate School Monterey, California 93940		8. CONTRACT OR GRANT NUMBER(s)
11. CONTROLLING OFFICE NAME AND ADDRESS Naval Postgraduate School Monterey, California 93940		10. PROGRAM ELEMENT, PROJECT, TASK AREA & WORK UNIT NUMBERS
14. MONITORING AGENCY NAME & ADDRESS (if different from Controlling Office) Naval Postgraduate School Monterey, California 93940		12. REPORT DATE Sep 1978
		13. NUMBER OF PAGES 94
		15. SECURITY CLASS. (of this report) Unclassified
		15a. DECLASSIFICATION/DOWNGRADING SCHEDULE
16. DISTRIBUTION STATEMENT (of this Report) Approved for Public Release; distribution unlimited		
17. DISTRIBUTION STATEMENT (of the abstract entered in Block 20, if different from Report)		
18. SUPPLEMENTARY NOTES		
19. KEY WORDS (Continue on reverse side if necessary and identify by block number) precipitate agglomeration weld cycle effects aluminum-magnesium alloy 5083-0 stress-corrosion susceptibility Liquified Natural Gas applications		
20. ABSTRACT (Continue on reverse side if necessary and identify by block number) The effects of multiple weld repairs on the aluminum-magnesium alloy 5083-0 as used in the primary self-supporting containment systems for Liquified Natural Gas Tankships were studied. The changes experienced by the material in micro-structure, mechanical properties and stress-corrosion susceptibility as a function of number of weld repairs were carefully		

DD FORM 1473
1 JAN 73
(Page 1)EDITION OF 1 NOV 65 IS OBSOLETE
S/N 0102-014-6601

1

UNCLASSIFIED

SECURITY CLASSIFICATION OF THIS PAGE (When Data Entered)

UNCLASSIFIED

SECURITY CLASSIFICATION OF THIS PAGE/When Data Entered

characterized and recorded. The results of these findings are discussed from both the metallurgical and the practical engineering standpoint.

ACCESSION for	
NTIS	White Section <input checked="" type="checkbox"/>
DDC	Buff Section <input type="checkbox"/>
UNANNOUNCED	<input type="checkbox"/>
J S I I C A I O N	
DISTRIBUTION/AVAILABILITY NOTES	
ORIGINAL	
A	

UNCLASSIFIED

SECURITY CLASSIFICATION OF THIS PAGE/When Data Entered

Approved for Public Release; distribution unlimited

THE EFFECTS OF MULTIPLE WELD
REPAIRS ON THE
ALUMINUM-MAGNESIUM ALLOY 5083-0

by

George R. Speight, Jr.
Lieutenant, United States Coast Guard
B.S., United States Merchant Marine Academy, 1970

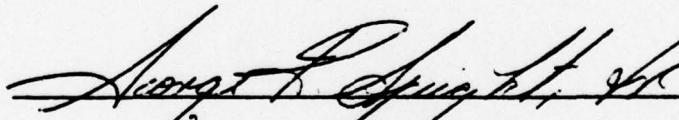
Submitted in partial fulfillment of
the requirements for the degree of

MASTER OF SCIENCE IN MECHANICAL ENGINEERING


from the

NAVAL POSTGRADUATE SCHOOL
September 1978

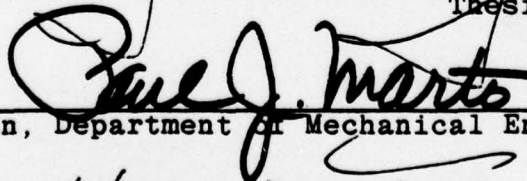
Author



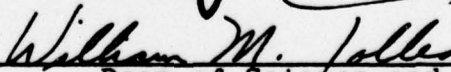
Approved by:



Thesis Advisor



Chairman, Department of Mechanical Engineering



Dean of Science and Engineering

ABSTRACT

The effects of multiple weld repairs on the aluminum-magnesium alloy 5083-0 as used in the primary self-supporting containment systems for Liquefied Natural Gas Tankships were studied. The changes experienced by the material in microstructure, mechanical properties and stress-corrosion susceptibility as a function of number of weld repairs were carefully characterized and recorded. The results of these findings are discussed from both the metallurgical and the practical engineering standpoint.

TABLE OF CONTENTS

ABSTRACT-----	4
LIST OF TABLES-----	7
LIST OF FIGURES-----	8
ACKNOWLEDGEMENT-----	12
I. INTRODUCTION AND BACKGROUND-----	13
A. WELDING IN SHIP CONSTRUCTION-----	13
B. ALUMINUM-MAGNESIUM ALLOYS-----	20
C. WELDING OF 5083-0 ALUMINUM-----	24
II. OBJECTIVES, PLANS AND PROCEDURES-----	33
A. OBJECTIVE-----	33
B. PLAN OF APPROACH-----	33
C. SOURCE OF MATERIALS-----	34
D. PROCEDURES-----	35
1. Welding of the Test Plates-----	35
2. Microscopy-----	37
a. Microscopic Examination in the "As-Polished" Condition-----	42
b. Microscopic Examination of Grain Size and Morphology-----	44
c. Microscopic Examination to Determine Differences in Preferential Precipitation at Grain Boundaries-----	44
3. Mechanical Characterization-----	45
a. Hardness Testing-----	45
b. Tension Testing-----	47
4. Resistance to Stress-Corrosion-----	47
a. Preparation of the Specimen-----	50

b. Stressing the Specimens-----	50
c. Sensitizing the Specimens-----	50
d. Immersion in Salt Water-----	50
III. RESULTS AND DISCUSSION-----	52
A. MICROSTRUCTURAL ANALYSIS-----	53
1. Microscopic Examination in the "As-Polished" Condition-----	53
2. Microscopic Examination of Grain Size and Morphology in the Etched Condition-----	60
3. Microscopic Examination Following the Phosphoric Acid Etch-----	67
4. Discussion of the Results of the Microstructural Analysis-----	72
B. MECHANICAL TESTING-----	74
1. Hardness Testing-----	74
2. Tension Testing-----	81
C. STRESS-CORROSION TESTS-----	84
IV. CONCLUSIONS-----	87
APPENDIX A ALLOY CHEMISTRY AND MECHANICAL PROPERTIES OF ALLOY 5083-0-----	90
APPENDIX B PREPARATION OF PSEUDO-SEA WATER-----	91
LIST OF REFERENCES-----	92
INITIAL DISTRIBUTION LIST-----	93

78 11 13 081

LIST OF TABLES

Table I.	Welding Parameters used in Fabrication of Test Plates-----	38
Table II.	Tension Test Data-----	79

LIST OF FIGURES

1. Photograph of the Coast Guard Secretary Class Cutter USCGC MORGENTHAU (WHEC-722). The superstructure of this vessel is of welded aluminum construction.-----15

2. Photograph of a Conch design "self-supporting" Liquified Natural Gas tank being loaded aboard ship at the Kaiser Fabricators Facility, Mobile, Alabama. The tank, one of five to be placed in the ship, is of all welded, 5083-0 aluminum construction.-----17

3. This figure represents the Aluminum-magnesium binary equilibrium phase diagram. The defined vertical region is the percentage range of magnesium found in the 5083-0 alloy. The schematic of the welded joint is introduced to give the reader a general idea of the peak temperatures experienced at various distances from the weld interface relative to the phase diagram.-----22

4. This figure shows curves which represent typical heating and cooling rates of a plate as a function of varying distances from the weld arc. The numbered curves correspond to the numbered locations shown on the schematic of the welded joint.-----26

5. Schematic of a MIG "gun" nozzle arrangement. The nozzle directs inert shielding gas to the weld joint. The copper contact tube completes the electrical circuit to the filler wire thereby allowing initiation and maintenance of the welding arc between the filler wire and the plate to be welded.-----30

6. Metal Inert Gas Welding Gun with push type wire feed. This schematic represents the general orientation of the "hand held" MIG "gun" for making down hand butt welds. The stationary control unit feeds shielding gas and filler wire at a preset rate to the gun while maintaining a predetermined power input. Water is supplied to the unit for cooling. The jog button allows the welder to manually feed wire for trimming prior to initiating the arc.-----31

7. (a) This figure represents the joint preparation performed prior to laying the first "downhand" or "flat" weld bead. After the first pass the plate is allowed to cool to a specified interpass temperature of 66°C (150°F) or less. The reverse side is backmilled to a minimum depth of 4.8 mm (3/16 inch) and then welded in the "flat" position. (b) The overlapping roots of the two passes. (c) The subsequent repair welds are made by grooving as shown, cooling to the temperature indicated above, and welding. The repair welds are made in a "flat" mode by changing plate sides with single pass repair.-----36
8. Schematic representing the areas of the welded test plates used for metallographic, mechanical and stress corrosion testing. The specimens were taken as near the center of the test plates and as close together as possible to avoid significant differences in cooling rates between specimens.-----39
9. The metallography specimens showing general dimensions. The indicated location array is shown to give the reader a general idea of the areas represented by the micrographs. A single specimen was used for both the "as-polished" and etched micrographs.-----41
10. This figure is intended to show the area representing the panorama of micrographs taken of the specimen after etching with the H₃PO₄ solution. The specimen is the same piece as shown in the left side of Figure 9.-----41
11. Photograph of the Bausch and Lomb Balpan Conference Microscope used in the microscopic analysis for this thesis.-----43
12. This figure represents the specimens used in determining the hardness profiles. The +'s indicate the locations where hardness data was compiled for each specimen. A series of hardness data was taken at 3 mm (0.118 inch) intervals along a line defining the midplane of the welded plate and at 3 mm from the midplane.-----46
13. Photograph of the Wilson Model 1-JR Rockwell Hardness Tester utilized in obtaining data for construction of the hardness profiles contained in this thesis.-----48
14. Schematic showing dimensions of the specimen used for tension testing for this thesis.-----49
15. Photomicrographs in the "as-polished" condition and in the "as-cast" weld metal of specimens subjected to the original two-pass weld only, 8 and 16 repair simulations-54

16. Photomicrographs taken of the "as-polished" specimen subjected to the original two-pass weld only. The locations represented are the interface (a), approximately 6 mm (b), 18 mm (c) and 27 mm (d) from the interface.-----55
17. Photomicrographs taken of the "as-polished" specimen subjected to 4 repair simulations. The locations represented are the interface (a), approximately 6 mm (b), 18 mm (c) and 27 mm (d) from the interface.--56
18. Photomicrographs taken of the "as-polished" specimen subjected to 8 repair simulations. The locations represented are the interface (a), approximately 6 mm (b), 18 mm (c) and 27 mm (d) from the interface.-----57
19. Photomicrographs taken of the "as-polished" specimen subjected to 12 repair simulations. The locations represented are the interface (a), approximately 6 mm (b), 18 mm (c) and 27 mm (d) from the interface.--58
20. Photomicrographs taken of the "as-polished" specimen subjected to 16 repair simulations. The locations represented are the interface (a), approximately 6 mm (b), 18 mm (c) and 27 mm (d) from the interface.--59
21. Photomicrographs in the etched condition of the specimens subjected to the original two-pass weld only (a), 8 (b) and 16 (c) repair simulations. The area represented in each of these micrographs is the "as-cast" weld metal.-----61
22. Photomicrographs taken of the etched specimen subjected to the original two-pass weld only. The locations represented are the interface (a) and approximately 6 mm (b), 18 mm (c) and 27 mm (d) from the interface.-----62
23. Photomicrographs taken of the etched specimen subjected to 4 repair simulations. The locations represented are the interface (a) and approximately 6 mm (b), 18 mm (c) and 27 mm (d) from the interface.--63
24. Photomicrographs taken of the etched specimen subjected to 8 repair simulations. The locations represented are the interface (a) and approximately 6 mm (b), 18 mm (c) and 27 mm (d) from the interface.--64
25. Photomicrographs taken of the etched specimen subjected to 12 repair simulations. The locations represented are the interface (a) and approximately 6 mm (b), 18 mm (c) and 27 mm (d) from the interface.--65

26. Photomicrographs taken of the etched specimen subjected to 16 repair simulations. The locations represented are the interface (a) and approximately 6 mm (b), 18 mm (c) and 27 mm (d) from the interface.--66
27. Photomicrographs of the specimen subjected to the original two-pass weld only. These micrographs were taken following etching with the H_3PO_4 solution.-----69
28. Photomicrographs of the specimen subjected to 8 repair simulations. These micrographs were taken following etching with the H_3PO_4 solution.-----70
29. Photomicrographs of the specimens subjected to 16 repair simulations. These micrographs were taken following etching with the H_3PO_4 solution.-----71
30. Hardness profiles for specimens subjected to the original two-pass weld only, 2 and 4 repair simulations. The solid line indicates data taken along the specimen centerline and the dashed line represents data taken along the line 3 mm from the centerline.-----75
31. Hardness profiles for specimens subjected to 6, 8 and 10 repair simulations.-----76
32. Hardness profiles of specimens subjected to 12, 14 and 16 repair simulations.-----77
33. This figure is a plot of the average tensile strengths recorded for specimens subjected to the original two-pass weld only, 4, 8, 12 and 16 repair simulations as a function of number of weld repairs.-----78

ACKNOWLEDGEMENT

The author wishes to express his sincere gratitude for the assistance provided by Professor Terry McNelley, as a friend and faculty advisor, throughout the course of this study. His untiring enthusiasm and suggestions, particularly in the final editing stage, resulted in the development of a clear and concise manuscript.

Special recognition is deserved by Captain William D. Markle, USCG; Commander Robert G. Williams, USCG; and LCDR Paul Pluta, USCG for their guidance and support in obtaining funding and information regarding this thesis.

Numerous consultations with Mr. Roy Edwards, Mechanical Engineering Department Technician, were of invaluable assistance in solving problems encountered in specimen preparation and photography.

Last but most certainly not least, the author is indebted to his wife, DeeJay, for her untiring assistance in metallographic preparation, photomicroscopy, and proofing. Without her assistance this thesis would not have known an expedient completion.

I. INTRODUCTION AND BACKGROUND

Technological advances have often grown from the throes of desperation. Such was the case experienced by the United States during the early years of World War II. With the American intervention into the war came an unprecedented need for merchant vessels to ferry supplies and troops to and from the war zones; ships were needed in great numbers and at a staggering rate. The fulfillment of this requirement came with the Liberty Ships. The 10,865 deadweight ton vessels were contrived as expendable and were expected to survive only one or two voyages in the hostile wartime environment. A total of 2,710 Liberty Ships were built between 1941 and 1944. The construction time for these vessels ranged from 150 days from keel-laying to launching for the first of the Liberties, the PATRICK HENRY, to the ROBERT E. PERRY which was launched only 4 days, 15 hours and 30 minutes following the laying of her keel [1].

A. WELDING IN SHIP CONSTRUCTION

The significance of welding in this area was aptly noted by Mr. Robert Young of the American Bureau of Shipping who stated: "Such speedy completion was made possible by welding large sub-assemblies elsewhere in the shipyards and then bringing them together for final assembly on the ways, a

technique daring in those days but today a standard ship-building method. Welding was a somewhat risky procedure since the first large 'all-welded' merchant ship had only been launched in 1937" [1].

The outstanding performance record of the Liberties, proved welding a reliable as well as efficient method for fabrication for large ships. Indeed, many of these ships have served 30 years! Welding remains today the primary joining technique used in large ship construction.

The industry has become quite adept in the fabrication of steel hulls by welding. Steels are the predominant materials used in large vessels; however, other materials are edging their way into areas where steels were once thought to be the only suitable material. With the need for larger and faster vessels has come a requirement for materials light in weight as well as strong. Also, cargoes have become more exotic and thus the requirements for their containment systems have become more stringent. Aluminum meets many of these requirements. In its pure form, aluminum is a ductile but weak material. Once alloyed it can be strong, tough and corrosion resistant while remaining light weight. Today aluminum is being used extensively in large marine applications from complete aluminum hull structures such as found in the ALCOA SEAPROBE to aluminum superstructures as can be found aboard the U. S. Coast Guard Secretary Class Cutters and many other naval vessels. Aluminum can be welded as readily as steel; of the 40 welding processes, aluminum is weldable by 32 [2].

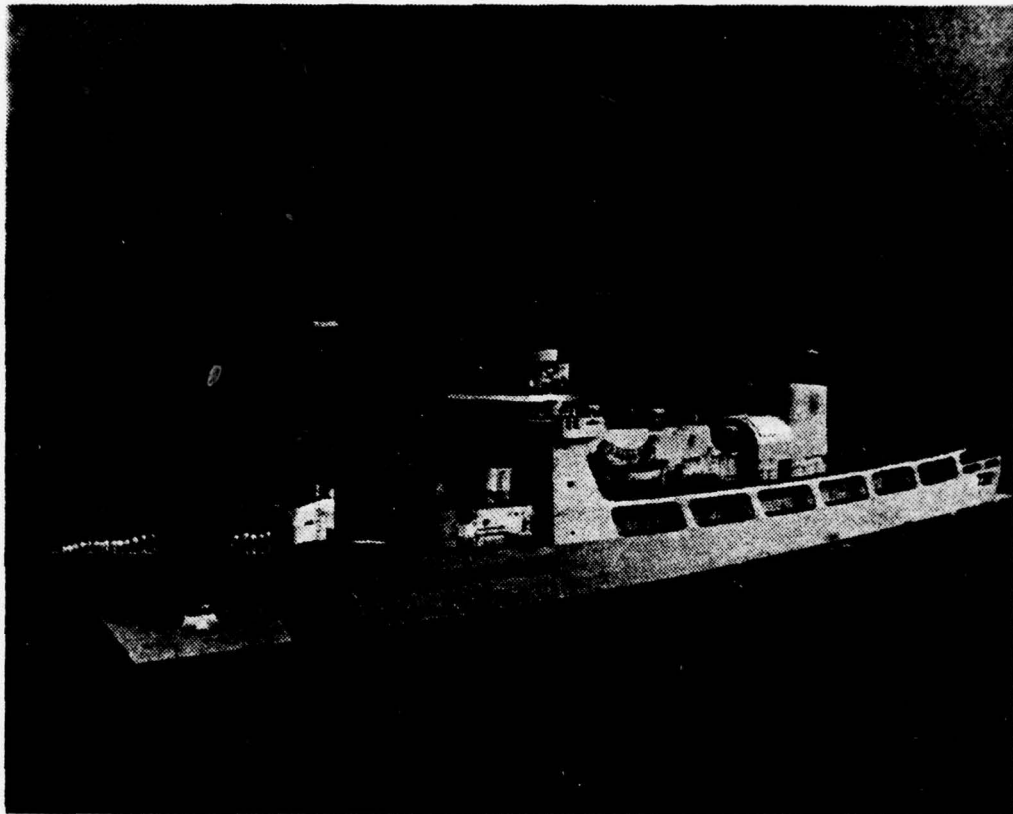


Figure 1. Photograph of the Coast Guard Secretary Class Cutter USCGC MORGENTHAU (WHEC-722). The superstructure of this vessel is of welded aluminum construction.

One of the most noteworthy uses of aluminum in recent years has come with the advent of the Liquified Natural Gas Tankships. At the time of this writing, there are 3 major designs of cryogenic LNG containment systems for tankships being built in the United States. Of the 3, two utilize 5083-0 aluminum alloy as the material from which the containment systems are fabricated. This particular alloy offers relative ease of welding and also possesses excellent properties at cryogenic temperatures making it especially suitable for LNG use.

The 3 major designs are 1) the Technigaz membrane containment system utilizing a stainless steel primary barrier, 2) the Moss-Rossenberg design spherical containment system, and 3) the Conch design prismatic containment system. The latter two systems utilize 5083-0 aluminum as the primary barrier. The first system is classed as a membrane or integral tank, while the spherical and prismatic designs fall in the "self-supporting" or semi-independent class. Both classes and each specific design offer advantages and disadvantages relative to one another. Since the purpose of this thesis is to discuss the effects of multiple weld repairs on aluminum welded joints such as are found in the latter class, our discussion in this section will be limited to the tank designs employing aluminum as the primary barrier. For a more in-depth discussion regarding each of the tank designs the reader is directed to Reference 3. Each of the 125,000 m³ LNG vessels contain 5 separate tanks. When utilizing a

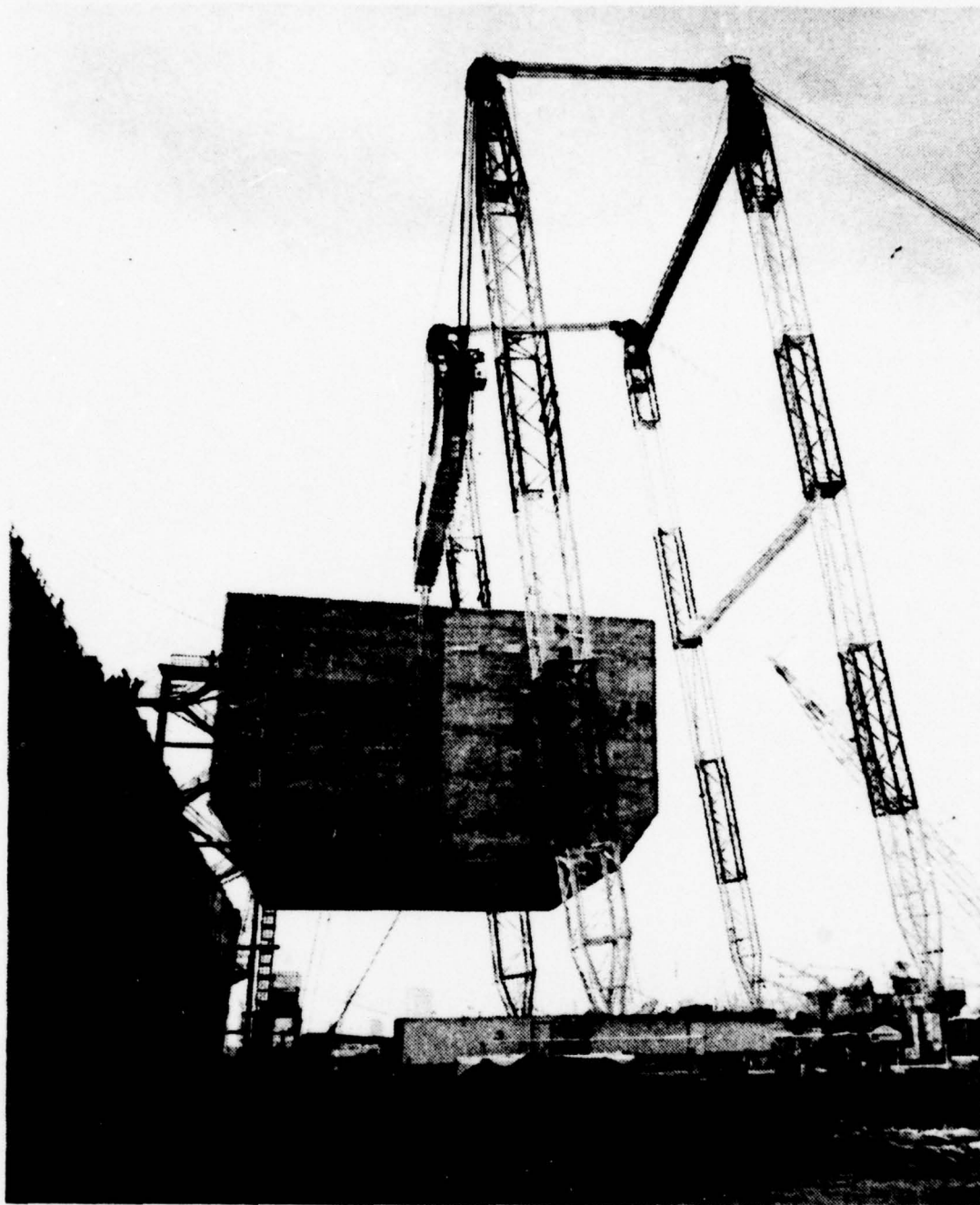


Figure 2. Photograph of a Conch design "self-supporting" Liquified Natural Gas tank being loaded aboard ship at the Kaiser Fabricators Facility, Mobile, Alabama. The tank, one of five to be placed in the ship, is of all-welded, 5083 aluminum construction. (Photograph compliments of Kaiser Aluminum Chemical & Sales Inc.)

self-supporting containment system, the tanks are fabricated independent of the vessel's hull and are not inserted into the hull until both the hull and tanks are complete. An important advantage of the self-supporting class systems is that tank construction may proceed independent of hull construction. This allows the tanks to be fabricated in controlled environments more advantageous for their specific fabrication requirements. A disadvantage in this design class is the requirement for heavy lift capabilities to move and insert the tanks into the hulls.

With this advantage and disadvantage in mind, attention may now be directed to the properties of aluminum which make it a primary choice for this application. Economic transportation of Natural Gas requires liquifaction. The gas, in a liquid state, is then loaded aboard ship at a temperature of -165°C (-265°F). These cryogenic temperatures require materials comprising the containment system to possess sufficient low temperature toughness to sustain loads without the possibility of unstable brittle fracture. Aluminum exhibits no embrittlement at these cryogenic temperatures whereas ferritic and martensitic steels do become embrittled at sufficiently low temperatures. In fact, the strength of aluminum actually is higher at low temperatures and there is little loss in ductility in comparison to room temperature.

The 5000 series aluminum-magnesium alloys are moderate to high in strength, allowing fabrication into large structures without excessive plate thicknesses and thus severe weight

penalty. Further, aluminum-magnesium alloys such as 5083 exhibit a density about one third that of stainless steel. Thus aluminum is a prime candidate for large structures which require lifting such as the "self-supporting" containment systems. In addition, aluminum is relatively low in cost and readily available; further, aluminum is non-sparking and corrosion resistant, extremely desirable characteristics in the marine transport of flammable products.

Those readers unfamiliar with the low temperature limitations of the carbon and alloy steels may wonder why it is not possible to fabricate the "self-supporting" tanks of the same material from which the hull is constructed. Great concern spread regarding the safety of all-welded hulls following the catastrophic hull failure of the T-2 Tanker SCHENECTADY while tied to the pier during the winter of 1941. It was found that the ductile-to-brittle transition temperature of structural steels being used at that time was within the range of service temperatures encountered by many vessels. Further, welded construction provides many stress concentrations due to weld defects. Subsequent work resulted in the development of the weldable high yield-strength alloy steels such as HY-80. The ductile-to-brittle transition temperatures of these steels, as welded, were pushed to temperatures below -50°C (-58°F), well outside the service temperatures experienced by most surface ships. This reduction in the ductile-to-brittle transition temperature was accomplished by modifications in alloy content and processing. The temperature of a Liquified

Natural Gas cargo, however, is approximately -165°C (-265°F), still lower than the ductile-to-brittle transition temperature of these newer steels. It is for this reason that austenitic stainless steels, nickel-base alloys or aluminum alloys are utilized in such cryogenic applications. Where "self-supporting" tanks are considered requiring structural scantlings and lifting, strong, but lightweight aluminum is the logical choice.

B. ALUMINUM-MAGNESIUM ALLOYS

The aluminum-magnesium alloys are non-heat treatable, solid-solution type alloys known as the 5000 series. Magnesium, whose atoms exist as a substitutional solid solution in the aluminum matrix, provides strengthening in this series allowing such alloys to exhibit moderate to high strengths. Alloys in this series are strengthened from an annealed condition by work hardening using such means as rolling, extruding or forging. The movement and multiplication of existing dislocations as a result of working the material, and interaction between stress fields of the dislocations and the strain fields created by the solute atoms, result in strengthening of these alloys by impeding further dislocation motion.

The magnesium content (weight percent) in the 5000 series varies from 0.5% to 5.0% depending upon the specific alloy. Aluminum alloy 5083, studied in this research, contains 4.0% to 4.9% magnesium as the primary alloy addition. Detailed alloy chemistry and mechanical property data are given in

Appendix A. In the unwelded annealed condition, this alloy exhibits a minimum yield strength of 18,000 psi (124.1 MPa), a minimum ultimate tensile strength of 40,000 psi (275.8 MPa), and 16% elongation in two inches. Magnesium is an effective strengthening agent when used by itself or in the presence of manganese. The reader may wonder then why not increase the amount of magnesium present to further increase the strength. Many of the 5000 series alloys were developed for marine applications which expose the material to rather severe corrosive environments. Because of such applications, care must be taken to formulate alloys for corrosion resistance as well as strength. For this reason, magnesium content must be limited. Figure 3 illustrates the equilibrium binary phase diagram for the aluminum rich range of the aluminum-magnesium system. The actual phase diagrams for specific alloys are complicated by the presence of numerous other elements which assist in strengthening and stabilizing the alloy. For the purpose of this discussion, however, the binary phase diagram will suffice. Also shown in the same figure is a schematic representation of a welded joint, showing peak temperatures experienced during welding relative to the phase diagram. For now, consider only the phase diagram. When an aluminum-magnesium alloy is processed by rolling, the alloy is worked primarily at temperatures in the range of stability of the aluminum-rich solid solution. Subsequent cooling to ambient temperatures leads to a "freezing in" of the magnesium in solid solution. The alloy may also be rolled at room temperature.

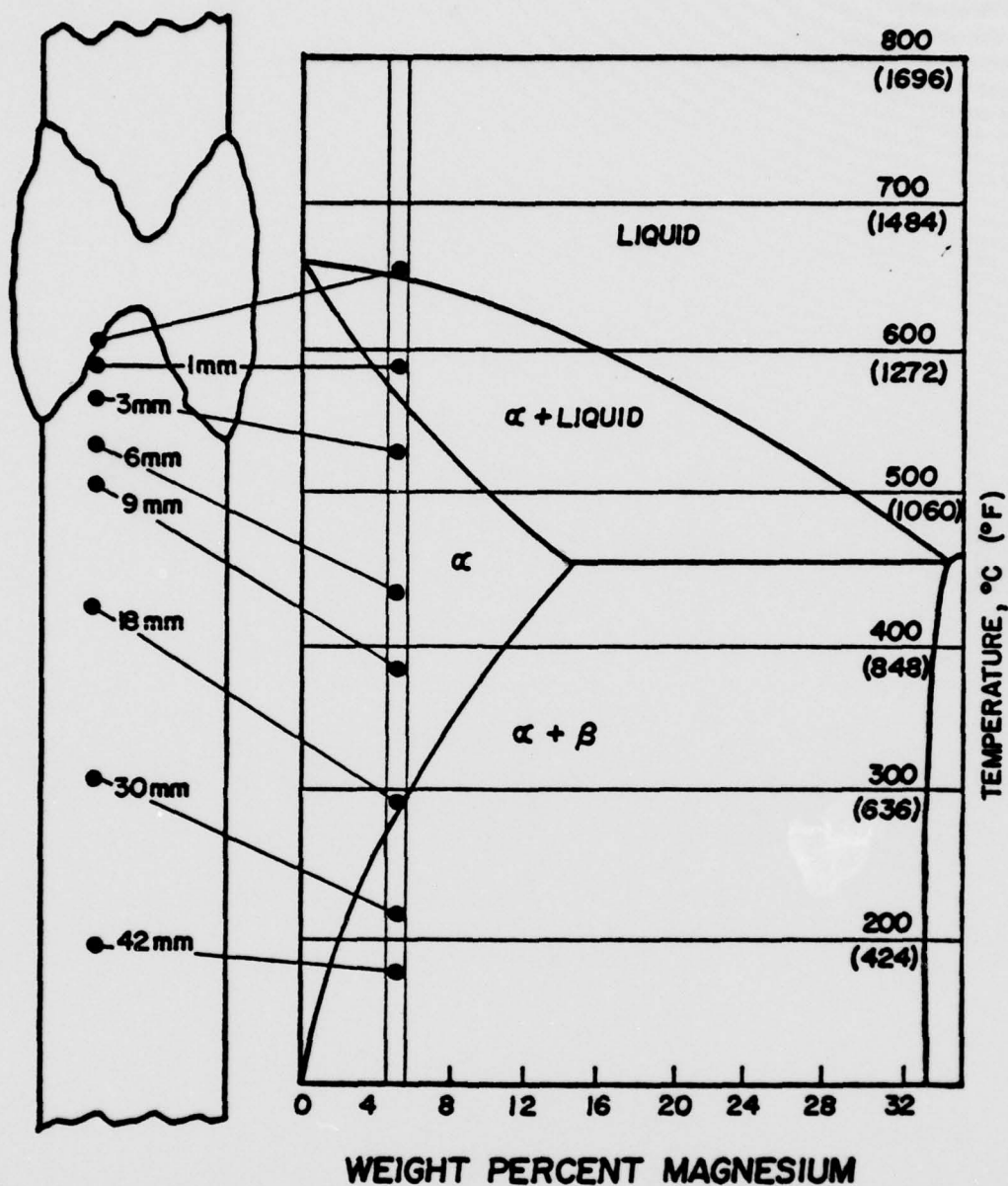


Figure 3. This figure represents the aluminum-magnesium binary equilibrium phase diagram. The defined vertical region is the percentage range of magnesium found in the 5083 alloy. The schematic of the welded joint is introduced to give the reader a general idea of the peak temperatures experienced at various distances from the weld interface relative to the phase diagram.

for strengthening. As illustrated on the phase diagram, the material is really in a metastable condition at ambient temperatures. Kinetic considerations, however, suggest that the transformation rate to the equilibrium two-phase alloy is slow and thus it is possible for the single phase alloy to remain essentially stable at ambient temperatures. However, aging may occur; this aging is manifested in the precipitation of the intermetallic compound Al_3Mg_2 (called β) from solid solution. Should precipitation occur preferentially at grain boundaries, problems may be encountered with stress-corrosion cracking or exfoliation. The phase diagram indicates that higher magnesium content leads to a greater degree of undercooling at ambient temperatures since the solvus temperature increases with increased magnesium content. This suggests a greater driving force for precipitation. Further, there is more magnesium which would want to precipitate, implying the possibility of a larger amount of grain boundary precipitation and hence more tendency for stress-corrosion cracking. The 5000 series alloys were formulated, based on many years of research, to avoid this problem. Service experience has shown that alloys containing less than 3.0% magnesium are unlikely to show evidence of stress-corrosion cracking at ambient temperatures [2]. Care must be taken, however, when using alloys whose magnesium content exceeds 3.0% and whose service environment exposes the material to moderately elevated temperatures for prolonged periods of time. The atom diffusion rate increases rapidly as temperature increases,

thus promoting more rapid aging and resultant susceptibility to stress corrosion.

C. WELDING OF 5083 ALUMINUM

5083 aluminum is a readily weldable alloy, weldable by any number of processes. As with any material however, a knowledge of the response of the material to thermal cycles is imperative to assure optimum performance of the welded joint.

The aluminum LNG containment systems previously discussed are fabricated utilizing the gas-metal arc welding process, metal-inert gas technique (MIG) as the primary joining method. The MIG technique will be discussed in more detail later in this section. At this point, let it suffice to say that MIG is a fusion welding process. During the welding process the material welded is subjected to peak temperatures ranging from above the liquidus to below the solvus depending on distance from the weld. Assuming a magnesium content of approximately 4.0 weight percent, reference may be made to Figure 3. Here is shown the relationship between points in the base metal at increasing distance from the weld interface and peak temperatures obtained. These temperatures are further related to the phase diagram. As is evident from this figure, areas of the welded plate experience temperatures representing each of the equilibrium phase regions for this alloy. Before further discussion of the effects of these peak temperatures,

one must also consider cooling rates experienced by this joint during the welding process. Figure 4 illustrates three important facts:

- 1) peak temperatures experienced decrease at increased distances from the center of the weld,
- 2) time to peak temperature increases at increased distances from the weld, and
- 3) cooling rate decreases at increased distances from the weld.

Aluminum exhibits a high rate of conduction heat transfer and therefore cooling rates are generally high. The portions of the metal exposed to temperatures above the liquidus are normally limited to the molten filler wire and a very small amount of the parent metal. The cooling rates here are also the highest. Because of this extremely short time at temperature, very little time is allowed for diffusion to occur to obtain equilibrium. The "as-cast" weld metal solidifies under non-equilibrium conditions and is therefore frozen as a multiphase alloy consisting primarily of grains of α and eutectic β . Thermodynamically, this microstructure would be unstable at room temperature. However, the rate of diffusion at room temperature is so slow that from a practical engineering consideration, the "as-cast" metal may be considered stable. The next portion of the welded joint considered is that portion whose peak temperatures carries it to just below the solidus temperature into the α phase region. If time at

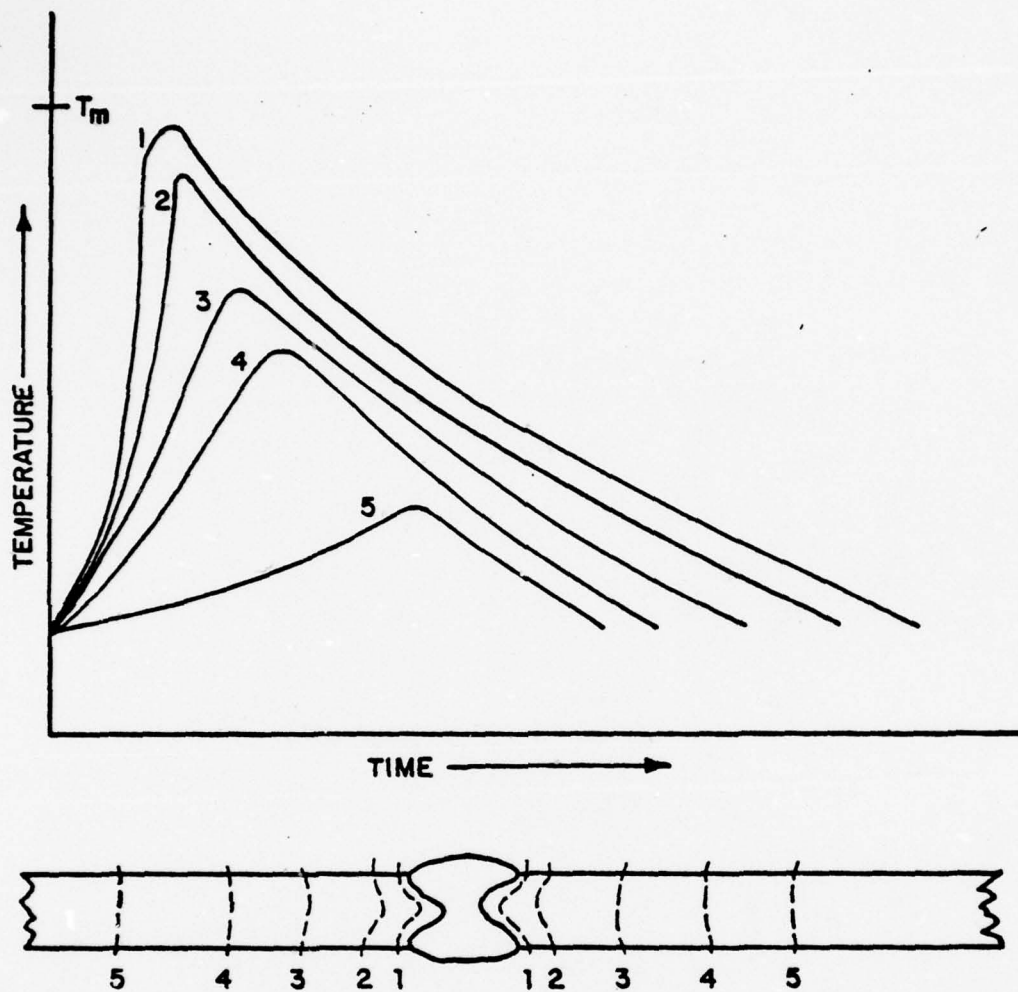


Figure 4. This figure shows curves which represent typical heating and cooling rates of a plate as a function of varying distances from the weld arc. The numbered curves correspond to the numbered locations shown on the schematic of the welded joint.

temperature is sufficient, all magnesium in that area will go into solid solution. In reality resolutioning will not be complete, again because of the very short time at temperature relative to diffusion rates. Since the material being welded is assumed to be a solid solution with relatively small amounts of second phase precipitates actually present, it may be assumed that the tendency would be to force the second phase into solution. Again, the time at temperature relative to the rate of diffusion through a solid is very short. Resolutioning will therefore be limited. As distance from the weld increases, the peak temperature attained is lower and there will be regions which reach peak temperatures below even the solvus temperature. All regions of the welded plate ultimately cool to ambient temperature. Those regions where magnesium was returned to the solid solution will again tend to have precipitation occur at temperatures below the solvus. Those larger particles not fully resolutioned will serve as nucleation sites for further precipitation and thus, ultimately, the larger particles will tend to grow at the expense of smaller particles. In addition, new precipitates may form at such preferred nucleation sites as grain boundaries. These are of special concern as such grain boundary precipitation generally leads to sensitization to stress corrosion. At distances further from the weld, the precipitate particles will be subject to the same tendency toward coarsening, but to a lesser extent given the relatively lower peak temperatures attained and the corresponding lower degree of atom mobility. As stated in the

previous section, 5083 contains from 4.0 to 4.9 weight percent magnesium. This rather high magnesium content may well create problems if the material is exposed to elevated temperatures for long periods of time. The service environment to which we have addressed ourselves thus far has been cryogenic in nature. The metal therefore will probably experience elevated temperatures during the welding process only.

The influence of increasingly large numbers of weld repairs is to increase the total time at temperature. Further, since precipitation will occur during only the cooling portion of the cycle, an increasingly large number of cycles experienced will likely have more effect than a total equivalent time at temperature but in a single cycle only.

In addition to these and other metallurgical considerations, one must be aware of the mechanical cycles the material witnesses during welding. As with any metal, aluminum undergoes thermal expansion and contraction with heating and cooling. Care must be taken to allow for these dimensional changes such that the material is not overly constrained. Excessive mechanical constraint may lead to large amounts of plastic deformation and even fracture of the weld metal.

Of no little importance to the increased popularity of aluminum as a structural material has been the development of efficient high speed welding techniques. Among those used in joining of moderate to thick sections, the Metal Inert Gas (MIG) technique has enjoyed the greatest popularity. The MIG process is a fusion arc process. MIG utilizes a consumable wire

electrode fed to the work from a reel through a series of rollers. The last contact the wire electrode makes with the MIG unit is through the contact tube. It is at this point that electrical contact is made with the wire. A schematic of the unit's nozzle is shown in Figure 5. The most important characteristic of this type of unit is its use of an inert gas to shield the area while welding. Because molten aluminum oxidizes rapidly when exposed to air, inert gas is necessary to shield the molten weld pool. Water vapor in the air can also be a problem; the water molecule can be reduced to hydrogen and oxygen in the arc. Hydrogen gas is soluble in liquid aluminum but relatively insoluble in solid aluminum. During solidification this can lead to porosity in the weld metal. The inert gas, usually an argon-helium mixture for aluminum-magnesium welding, is fed to the work piece through the MIG "gun" nozzle as shown in Figure 5. Figure 6 is a schematic of a hand held MIG "gun". The automatic or machine welding units are comprised of essentially the same components mounted on a tractor which may utilize a groove follower guide.

Many variables must be considered when attempting to determine peak temperatures and cooling rates experienced by metals being welded. Some of the more important ones are: density of the material; plate temperature prior to welding; specific heat of the material and welding speed. Power input, and thus heat input, is a function of current density and electrode potential. The rate of conduction heat transfer is a function of the heat capacity, thickness, density and

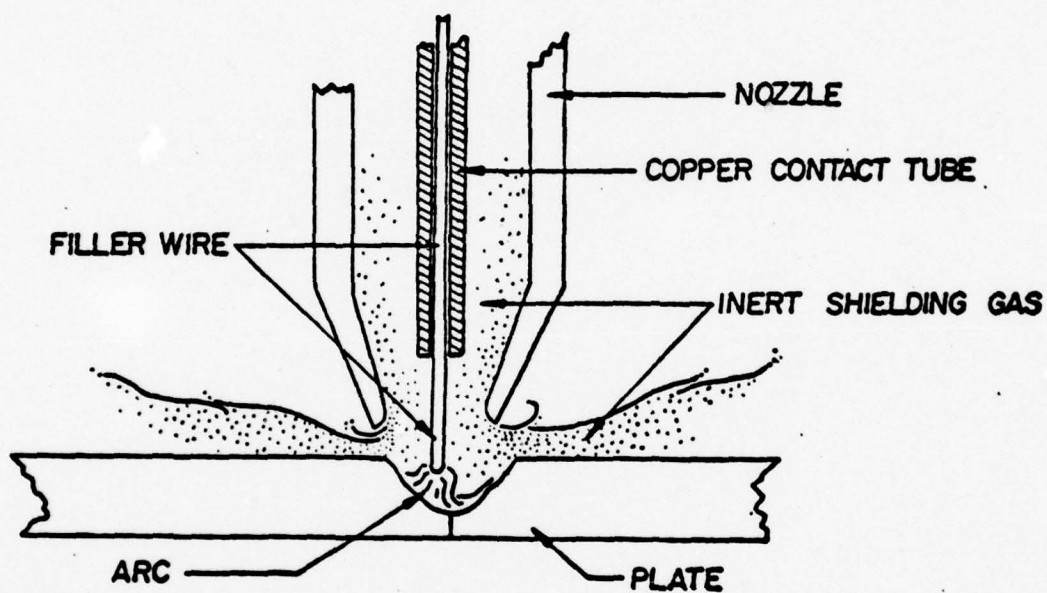


Figure 5. Schematic of a MIG "gun" nozzle arrangement. The nozzle directs inert shielding gas to the weld joint. The copper contact tube completes the electrical circuit to the filler wire thereby allowing initiation and maintenance of the welding arc between the filler wire and the plate to be welded.

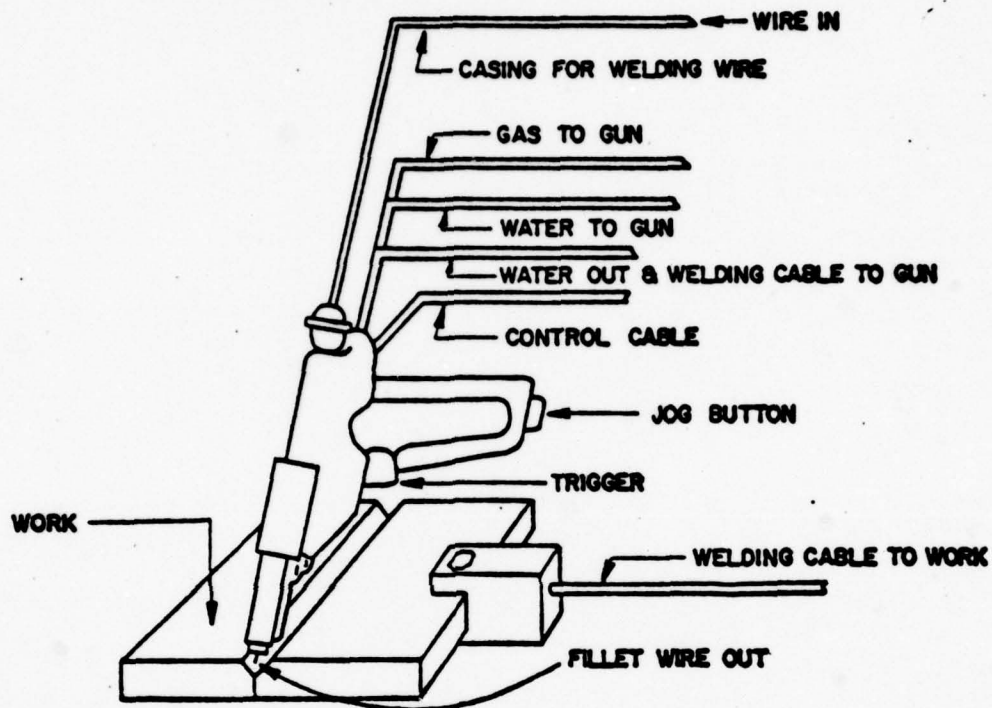


Figure 6. Metal Inert Gas Welding Gun with push type wire feed. This schematic represents the general orientation of the "hand held" MIG "gun" for making down hand butt welds. The stationary control unit feeds shielding gas and filler wire at a preset rate to the gun while maintaining a predetermined power input (heat input). Water is supplied to the unit for cooling. The jog button allows the welder to manually feed wire for trimming prior to initiating the arc. (Figure adapted from Reference 2.)

pre-weld temperature of the material being welded. These variables may be combined into a linear formula relating each of these to the peak temperatures experienced at a specific distance from the molten weld pool. This relationship, as found in Reference 4 as equation 3.1, is:

$$\frac{1}{T_p - T_o} = \frac{4.13\rho CtY}{H_{net}} + \frac{1}{T_m - T_o}$$

where T_p is the peak or maximum temperature ($^{\circ}\text{C}$) at a distance Y (mm) from the weld interface, T_o is the uniform temperature ($^{\circ}\text{C}$) of the plate prior to welding, T_m is the melting temperature ($^{\circ}\text{C}$) of the metal being welded, H_{net} is the net energy input which is further given by fEI/V , where E and I are the electrode potential (volts) and current (amps) respectively, f is the heat transfer efficiency and V is the travel speed (mm/s) of the arc. The density of the material being welded (g/mm^3) is ρ , C is the specific heat of the solid metal being welded ($\text{J/g}^{\circ}\text{C}$), and t is the thickness of the plate being welded (mm).

II. OBJECTIVES, PLANS, AND PROCEDURES

A thorough knowledge of a material's limitations as well as properties is imperative to the designer using that material. This becomes paramount when the material is to be fabricated into a structure where failure of the structure could result in catastrophic losses. Welded structures are subjected to severe thermal cycles each time a weld is made. Determination of a material's suitability for an intended application where welding is used necessitates a thorough knowledge of the engineering effects of microstructural changes in response to these thermal cycles.

A. OBJECTIVE

Weld repairs, and even multiple weld repairs, are often necessary in welded structures. Multiple weld repairs in a single location of a structure subjects that location to a new thermal cycle each time a weld repair is made. The objective of this research is to simulate and then characterize the effects of multiple weld repairs on welded joints made in 5083 aluminum alloy of the "O" (annealed) temper.

B. PLAN OF APPROACH

To meet the objective set forth in the previous paragraph, this research was conducted in three parts:

- 1) Effects of multiple weld repairs on microstructure
- 2) Effects of multiple weld repairs on mechanical properties
- 3) Effects of multiple weld repairs on resistance to stress-corrosion cracking.

The procedures followed, results and implications derived in each of these parts will be discussed in the remainder of this thesis.

C. SOURCE OF MATERIALS

Materials used in this investigation were obtained from the Center for Technology, Kaiser Aluminum and Chemical Sales Inc., Pleasanton, California. The desire to simulate the effects of multiple weld repairs upon this specific alloy without the introduction of additional variables required such simulation be performed under laboratory conditions. So that a proper correlation could be made between these tests and actual structures it was, however, desirable to duplicate industrial welding practice and materials as closely as possible. Thus, it was necessary to acquire material of not only the proper alloy but the proper temper as well. Due to cost constraints and material availability, 5083 aluminum alloy in the H-321 temper was purchased. This material was then exposed to a production-type controlled anneal at the Pleasanton facility. This anneal consisted of a controlled heating to a temperature of 454°C (850°F), followed by a two hour soak at

temperature and a controlled furnace cool-down cycle. This annealing procedure resulted in an "O" temper, the softest commercial temper of wrought aluminum plate. The welding, or filler, wire used in fabrication of the test plates was of 5183 type and was also obtained from Kaiser Aluminum.

D. PROCEDURES

The various procedures used in this characterization approximated standard industrial practices and tests as closely as possible. Details regarding specimen preparation and the individual tests are discussed in the following sub-sections.

1. Welding of the Test Plates

The plates to be welded were all cut from the same rolled plate. Each plate was cut with its greatest dimension oriented in the direction of rolling. The plates to be welded measured approximately 254 x 610 x 12.7 millimeters (10 x 24 x 0.5 inches). The plates were then annealed from the H-321 temper to the "O" temper. All plates were then degreased using acetone solvent. Machine beveling was performed along the greatest dimension on one edge of each plate to provide edge preparation as shown in Figure 7(a). After the plates were welded on one side in the flat (downhand) position they were turned over, backmilled and again welded in the flat position (Figure 7b). A total of nine (9) plates were welded in this fashion. One of the nine plates was set aside to be used to characterize

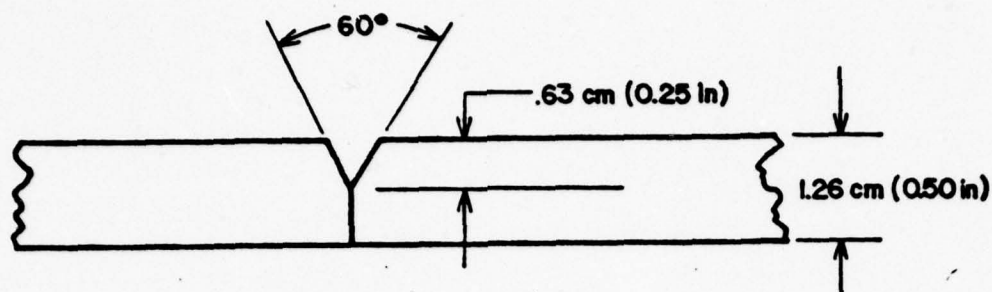


Figure 7 (a)

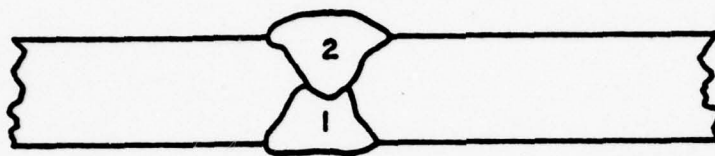


Figure 7 (b)

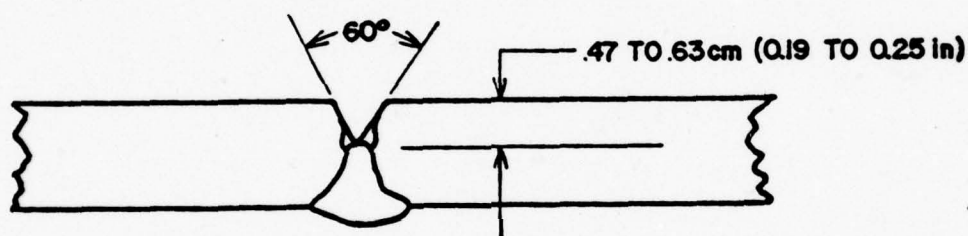


Figure 7 (c)

Figure 7. (a) This figure represents the joint preparation performed prior to laying the first "downhand" or "flat" weld bead. After the first pass the plate is allowed to cool to a specified interpass temperature of 66°C (150°F) or less. The reverse side is backmilled to a minimum depth of 4.8 mm ($3/16$ inch) and then welded in the "flat" position.

(b) The overlapping roots of the two passes.

(c) The subsequent repair welds are made by grooving as shown, cooling to the temperature indicated above, and welding. The repair welds are made in a "flat" mode by changing plate sides with each single pass repair.

the original two-pass welded joint. The remaining eight plates were subjected to weld repair simulations. Each repair simulation was performed by welding after preparation as shown in Figure 7(c). The first of the remaining eight plates was subjected to this repair simulation twice, first on one side then on the other with each weld being performed in the flat position. The second plate underwent four repair simulations (two repairs on each side). Plates three through eight underwent a progression of six through sixteen repair simulations, respectively, with an equal number of weld repairs on each side. The original and simulated repair welds were made by the Automatic Gas Metal Arc Process, Metal Inert Gas Technique, utilizing the welding parameters as shown in Table I.

After welding, the test plates were radiographed and reviewed in accordance with procedures set forth in Section VIII, Division 1 of the 1971 edition of the ASME Code to assure a minimum radiographic weld quality commensurate with those required for commercially built pressure vessels. The location of subsequent test specimens relative to the test plate were as shown in Figure 8; the specimens were taken as near the center of the plate as practicable to avoid significant differences in cooling rate due to end effects.

2. Microscopy

The microstructural comparison of the test specimens was divided into 3 major categories as follows:

Table I. Welding Parameters used in
Fabrication of Test Plates.

	ORIGINAL WELD & REPAIR WELD
WELDING PROCESS	Mechanical Gas Metal Arc
ATMOSPHERE	75% Helium & 25% Argon shielding gas
SHIELDING GAS FLOW	80 Cubic feet per hour
NOZZLE OPENING DIAMETER	0.625 inches
TYPE POWER SOURCE	Drooping Characteristic
CURRENT TYPE	Direct Current Reverse Polarity
ELECTRODE POTENTIAL	Negative
BASE METAL	5083-0 Aluminum
BASE METAL THICKNESS	0.50 inch
FILLER METAL	5183 Aluminum
FILLER METAL DIAMETER	1/16 inch
WELDING POSITION	Downhand (Flat)
AMPERAGE	250-260 Amps
VOLTAGE	33-34 Volts
RATE OF WIRE FEED	395 inches per minute
MACHINE TRAVEL SPEED	18 to 22 inches per minute

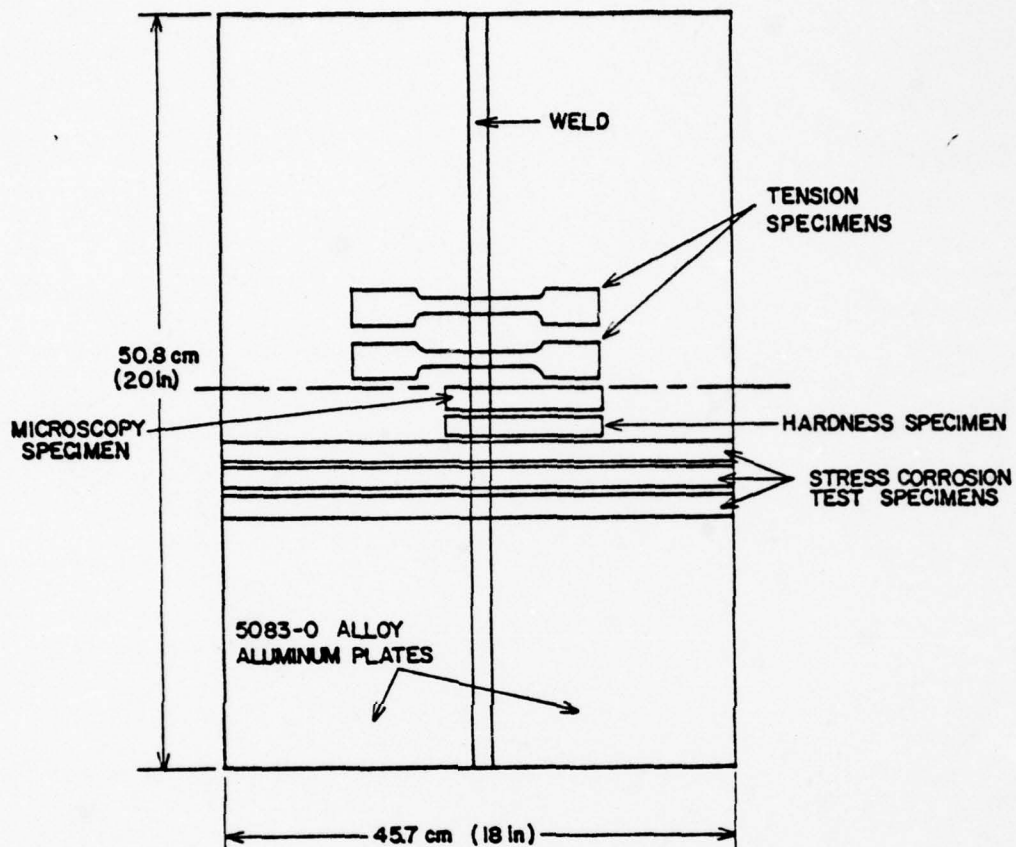


Figure 8. Schematic representing the areas of the welded test plates used for metallographic, mechanical, and stress corrosion testing. The specimens were taken as near the center of the test plates and as close together as possible to avoid significant differences in cooling rates between specimens.

- 1) Examination in the "as-polished" condition to compare differences in precipitates between the specimens.
- 2) Examination in the etched condition to compare differences in grain size and morphology.
- 3) Examination in the etched condition to examine for preferential precipitation at the grain boundaries.

The procedures used in the preparation for microscopic examination consisted of machining the specimens, grinding, polishing and then etching where necessary. All three categories of microstructural examination utilized the same specimen. This assured that the examination in each of the categories was performed on a specimen subjected to the same thermal history.

Each specimen was first machined from the test plate such that the surface to be examined was in a plane defined by the short and long transverse directions of the test plate. The face of the specimen was machined to a surface finish of $\sqrt{65}$. After machining, the specimens were sectioned as shown in Figure 9. This sectioning was necessary to adapt the specimen to the polishing equipment in the Material Science Laboratory at the Naval Postgraduate School. The specimens were then ground using O-grit silicon carbide paper. The next two polishing steps utilized an aluminum oxide slurry of O-grit and 15 μ m-grit, respectively, on a rotating polishing wheel with a wheel speed of 550 rpm. The final polishing

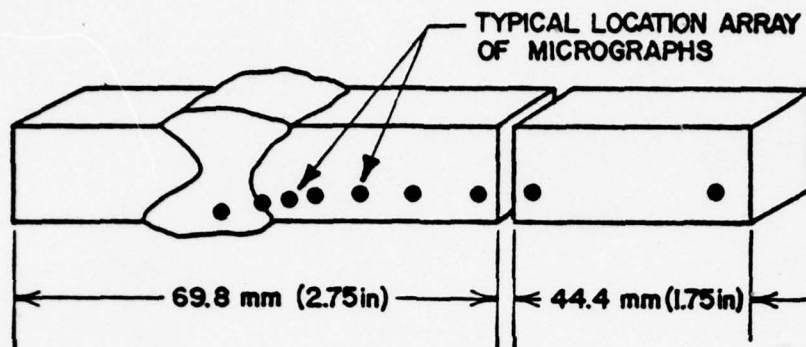


Figure 9. The metallography specimens showing general dimensions. The indicated location array is shown to give the reader a general idea of the areas represented by the micrographs. A single specimen was used for both the "as-polished" and etched micrographs.

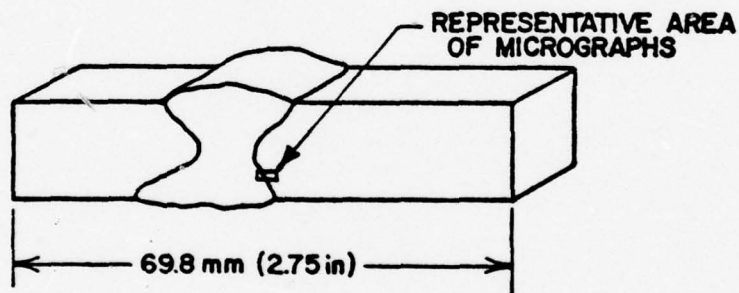


Figure 10. This figure is intended to show the area representing the panorama of micrographs taken of the specimen after etching with the H_3PO_4 solution. The specimen is the same piece as shown in the left side of Figure 9.

step utilized a rotating polishing wheel with a wheel speed of 170 rpm and "MAGOMET" magnesium oxide polishing compound. The magnesium oxide was applied to the polishing wheel in a paste form with continuous dilution of the abrasive paste with distilled water as the final polishing stage reached completion. The specimens were rinsed with tap water followed by ultrasonic cleaning and a final rinse with distilled water between each polishing step. This polishing procedure was performed on each specimen prior to examination in the as polished condition and between etchings as necessary.

All optical microscopic examination and photomicroscopy was performed utilizing a Bausch and Lomb Balpan Conference Microscope located in the Microscopy Laboratory at the Naval Postgraduate School. Figure 11 is a photograph of that photomicroscope.

a. Microscopic Examination in the "As-Polished" Condition

Microscopic examination in the "as-polished" condition was performed on specimens from the original two-pass welded joint and on specimens representing 4, 8, 12 and 16 repair simulations. The specimens were viewed and photographed at a magnification of 100 diameters without the aid of optical filters or analysers. The film used in recording the microscopic analysis in the "as-polished" condition was Polaroid Type 57 (3000 ASA) Positive Film. Typical exposure setting was 1/30 of a second. Examination was conducted to study differences in insoluble precipitates among the specimens.

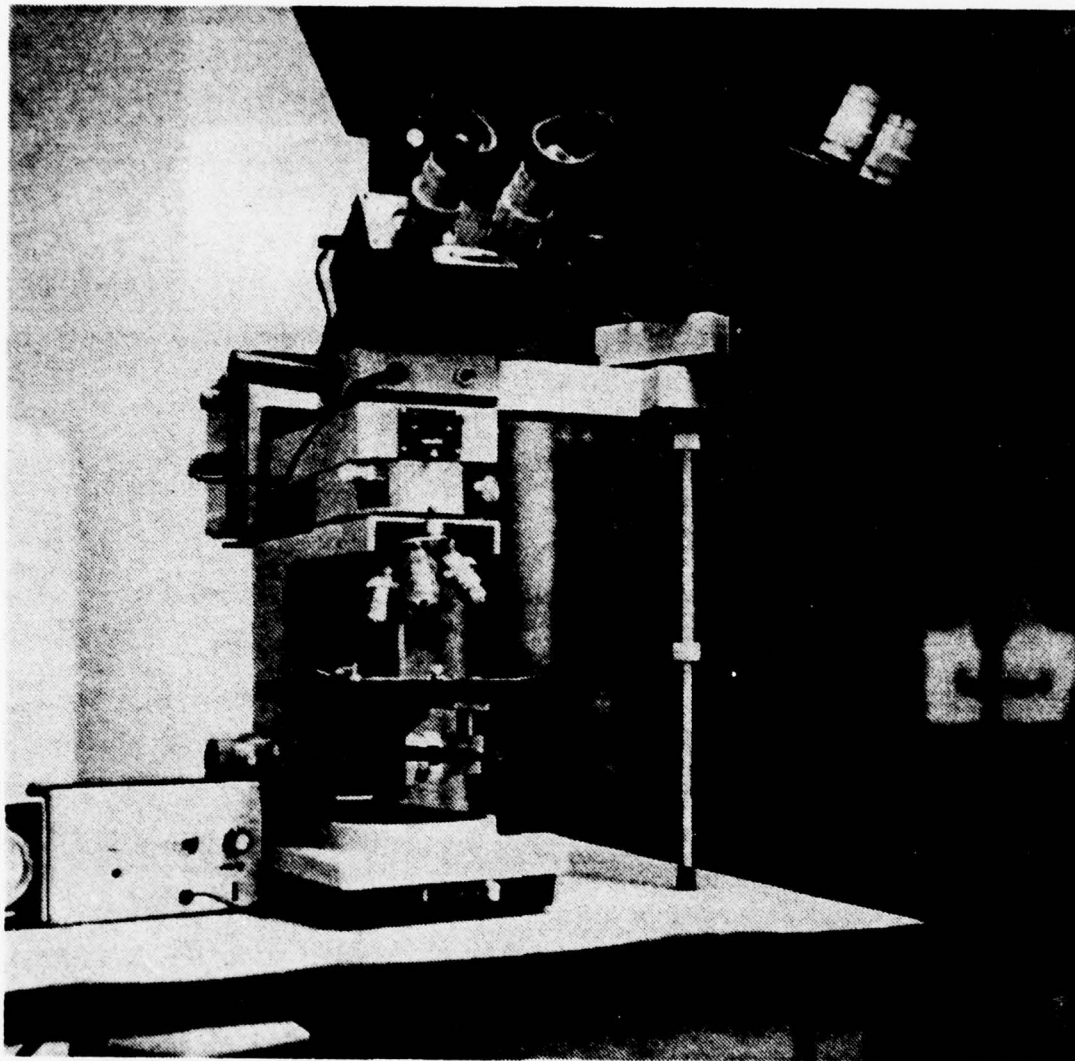


Figure 11. Photograph of the Bausch and Lomb Balpan Conference Microscope used in the microscopic analysis for this thesis.

b. Microscopic Examination of Grain Size and Morphology

After recording data in the "as-polished" condition, the specimens were etched and examined to investigate grain size and morphology. The specimens examined were the same as those listed above. A slight modification of etchant #12, as found on page 124 of Reference 5, was used. The etching solution consisted of the following:

40 ml CrO_3 solution (3 grams CrO_3 to each 10 ml H_2O)
30 ml HCL
2.5 ml 48% HF
2.5 ml H_2O
65 ml HNO_3

The etchant was poured onto the specimen until the surface to be examined began to exhibit a frosty appearance. The specimen was then rinsed and swabbed with alcohol to desmut followed by a distilled water rinse and dry.

c. Microscopic Examination to Determine Differences in Preferential Precipitation at Grain Boundaries

Microscopic examination to determine differences in preferential precipitation at grain boundaries was performed on specimens representing the original two-pass welded joint and 8 and 16 repair simulations. Examination was performed following repolishing and etching with a solution of 10 ml H_3PO_4 (85%) and 90 ml of water. This solution is referred to as etchant #8 by the Metals Handbook [5]. The

specimens were immersed in the solution, which had been preheated to a temperature of 50°C (122°F), for a period of 4 minutes. The specimens were then rinsed and dried with an electric blowdryer. Microscopic examination and photomicroscopy were performed at a magnification of 200 diameters without the aid of optical filters or analysers. The film used in obtaining these photomicrographs was Polaroid Type 57 (3000 ASA) Positive Film. An exposure time of 1/30 of a second was used. Micrographs of each of the specimens were taken representing an area of approximately 2 mm (0.08 inches) in length, starting with a location in the "as-cast" weld metal approximately 0.5 mm (0.02 inches) from the weld interface. Figure 10 shows the general area examined.

3. Mechanical Characterization

Mechanical characterization was conducted utilizing two test methods: hardness testing and tensile testing. Sample preparation and methods of data collection are discussed in the following subsections.

a. Hardness Testing

Hardness tests were performed on specimens taken from each of the nine test plates. Figure 12 shows the locations where hardness data was taken relative to the individual specimens. The specimens were prepared by machine surfacing to a surface finish of $\sqrt{65}$ followed by a final sanding on 600-grit wet/dry paper using kerosene lubricant.

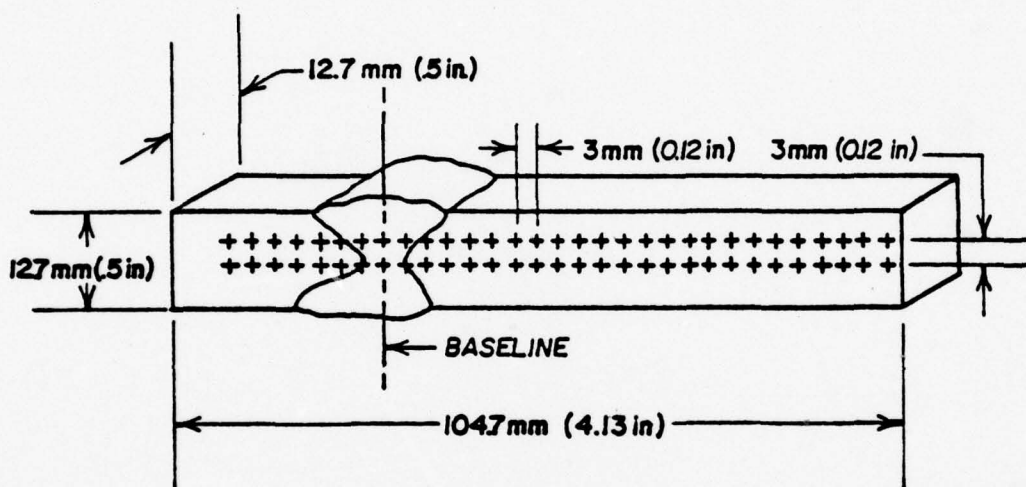


Figure 12. This figure represents the specimens used in determining the hardness profiles. The +'s indicate the locations where hardness data was compiled for each specimen. A series of hardness data was taken at 3 mm (0.118 inch) intervals along a line defining the midplane of the welded plate and at 3 mm from the midplane.

Data were obtained on a Wilson Rockwell Hardness tester (shown in Figure 13) utilizing a 1.59 mm (1/16 inch) ball penetrator with a 60 kilogram (132.2 pound) load. All data were taken on the Rockwell F scale.

b. Tension Testing

Tension tests were performed on two specimens from each of the nine test plates. The specimens were prepared by machining to dimensions as shown in Figure 14. Prior to actual testing, two-inch gage marks were placed on each side of the specimens to allow calculation of elongation. Testing was performed at an extension rate of 1.27 mm (0.05 inches) per minute on an Instron Model TTD Mechanical testing machine located in the Material Science Laboratory at the Naval Postgraduate School.

4. Resistance to Stress Corrosion

Three specimens were taken from plates representing the original weld, 4, 8, 12 and 16 repair simulations. The first specimen from each test plate was subjected to an applied stress followed by immersion in a salt water solution. The second specimen from each test plate was sensitized, then stressed, followed by immersion in a salt water solution. The third and final specimen from each of the nine test plates was stressed and then sensitized, followed by immersion in a salt water solution. The following paragraphs discuss details of the test steps.

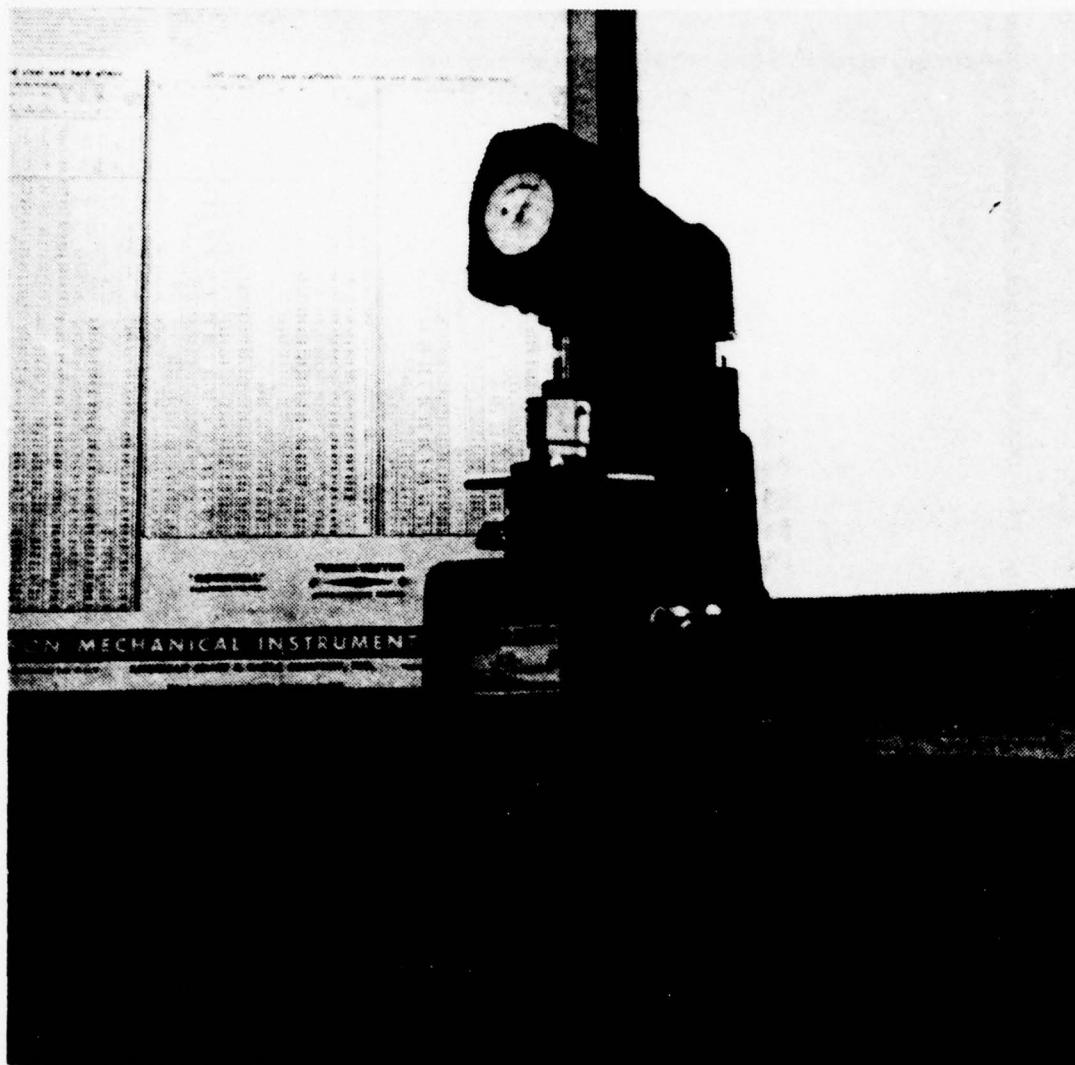


Figure 13. Photograph of the Wilson Model 1-JR Rockwell Hardness Tester utilized in obtaining data for construction of the hardness profiles contained in this thesis.

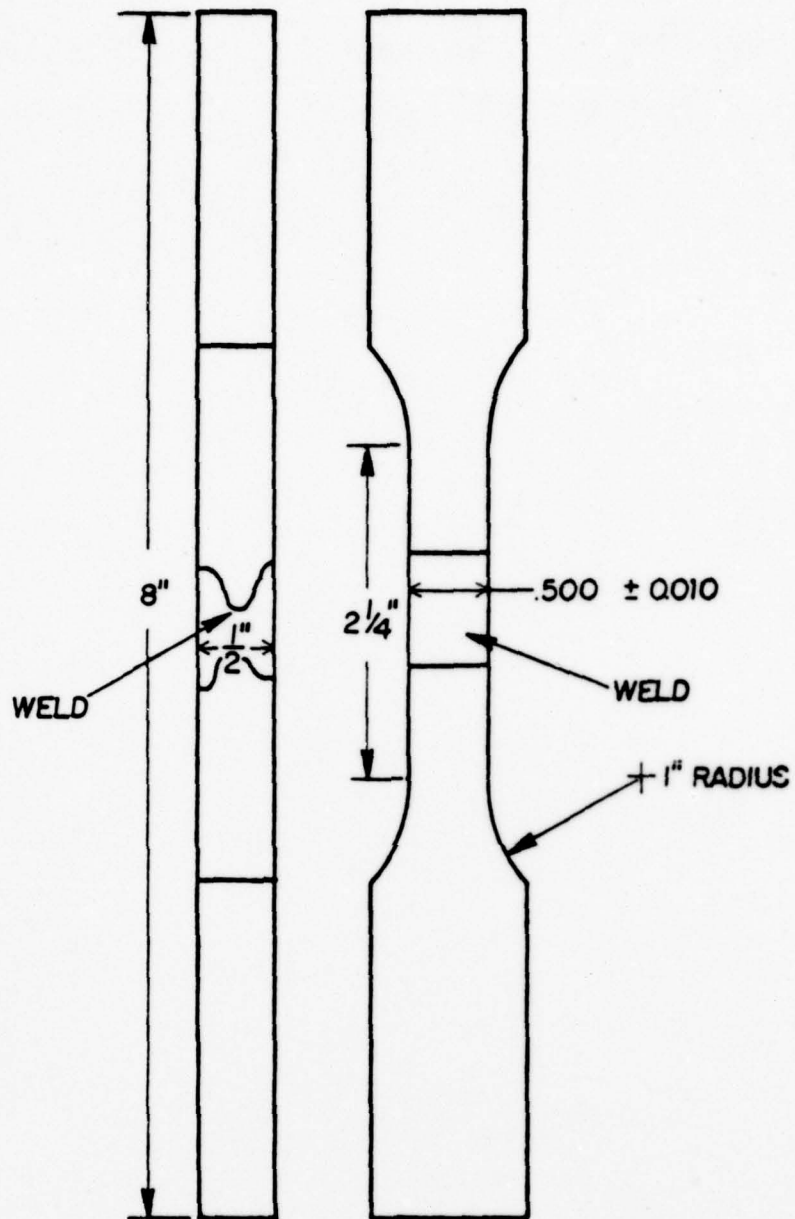


Figure 14. Schematic showing dimensions of the specimen used for tension testing for this thesis.

a. Preparation of the Specimens

Three specimens were taken from each of the test plates as shown in Figure 8 with dimensions of 12.7 x 12.7 x 457 mm (0.5 x 0.5 x 18 inches). The ends of the specimens were drilled to accommodate a 2.5 mm (0.10 inch) diameter steel stressing bolt.

b. Stressing the Specimens

The specimens were subjected to a guided face bend of 64 mm (2.5 inches) radius. After bending, the stressing bolt was passed through the ends of the specimen and tightened to return the specimen radius to 64 mm thereby placing the weld face in a constant state of tension. The stressing bolts remained in place throughout the remainder of the experiment.

c. Sensitizing the Specimens

The specimens were sensitized by subjecting them to a controlled temperature of 125°C (257°F) for a period of one week followed by a furnace cool. This sensitizing procedure simulates, in effect, prolonged exposure of the material to ambient temperatures. The sensitizing temperature is below a temperature at which magnesium in the alloy would tend to go entirely into solution.

d. Immersion in Salt Water

The specimens were subjected to a total immersion in a pseudo-salt water solution prepared using the formula and

procedure developed by Kester et al. [6]. The composition of this solution may be found in Appendix B. The specimens were immersed for a period of 14 days prior to examination for evidence of stress-corrosion cracking.

III. RESULTS AND DISCUSSION

Prior to discussion of the effects of multiple weld repairs, it is appropriate to reiterate the properties exhibited by the material in the unwelded condition. The material used in this experimentation was 5083 aluminum of the "O" temper. This material is a non-heat treatable, solid solution alloy strengthened by solute elements when in the annealed condition. Further strengthening depends upon the degree of strain hardening to which the material is exposed. Since the material used in this experimentation was annealed prior to welding, there would be no large changes anticipated in tensile strength, relative to the original unwelded plate, as a result of the heat input during welding. There will be, however, microstructural change as a result of the thermal cycles imposed upon the material as a result of welding. The degree of microstructural response, or manner in which this response would be manifest as a result of 16 weld repairs, was unknown prior to completion of the various tests. It should be noted that with the repeated heating and cooling cycles inherent in any welding process also comes expansion and contraction of the material. This expansion and contraction, particularly where large structures constrain the repair area, may provide for a significant degree of strain hardening. Thus care must be taken in the interpretation of experimental results and especially when designing repair procedures for welded structures.

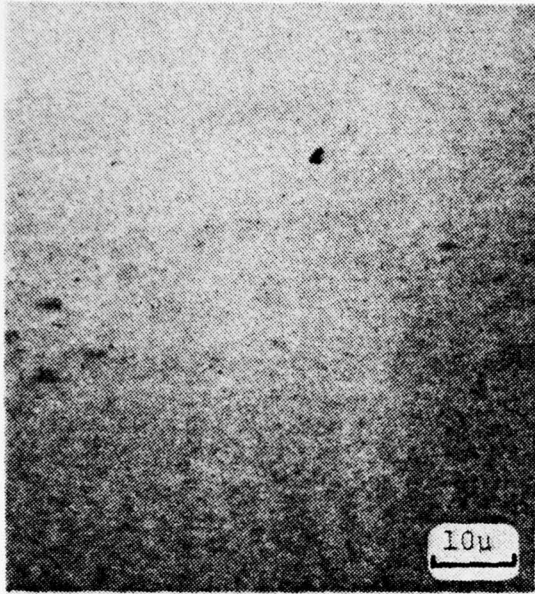
A. MICROSTRUCTURAL ANALYSIS

Microstructural examination was performed in the "as-polished" condition, after etching with modified reagent #12, and after etching with phosphoric acid (H_3PO_4). Specific metallographic procedures were discussed in Section II.B. The results of such examination are given in the following paragraphs.

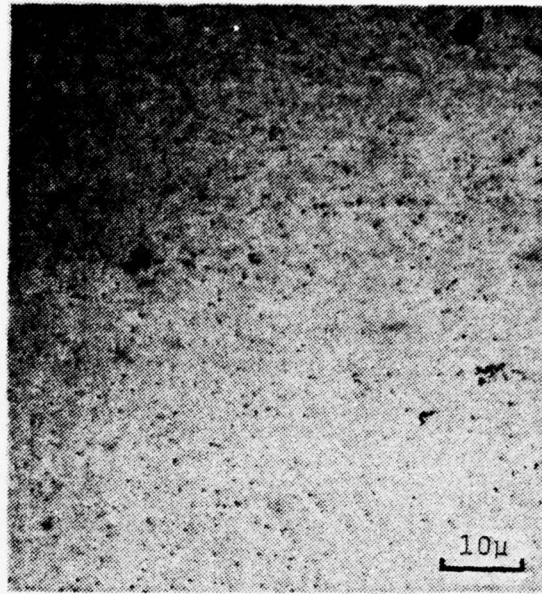
1. Microscopic Examination in the "As-Polished" Condition

Selected photomicrographs of the original two-pass weld, 4, 8, 12 and 16 repair simulations in the "as-polished" condition and at similar locations on each specimen are shown in Figures 15 through 20.

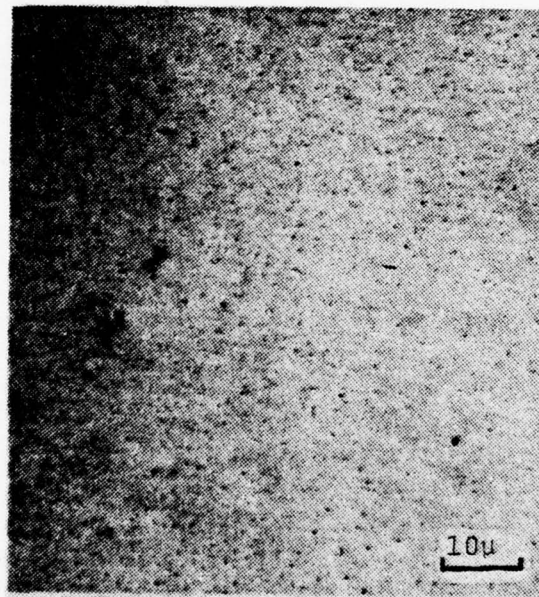
Figure 15 shows photomicrographs of the "as-cast" weld of the specimens consisting of the original two-pass weld and eight and sixteen repair simulations. It is evident from these micrographs that little difference may be found in the microstructure of the "as-cast" weld metal as a function of number of weld repairs. This result is to be expected. Since the repair simulations were effected by removing the previous weld metal and redepositing new weld metal, utilizing the same essential welding parameters, we have performed essentially the same procedure with each repair. Thus the deposited weld metal in the sixteenth repair simulation should duplicate that deposited in the original weld. The differences in the specimens as a function of number of repair simulations begins at the weld interface. Figures 16 through 20 are



original two-pass weld



8 repair simulations



16 repair simulations

Figure 15. Photomicrographs in the "as-polished" condition and in the "as-cast" weld metal of specimens subjected to the original two-pass weld only, 8 and 16 repair simulations. (100X)

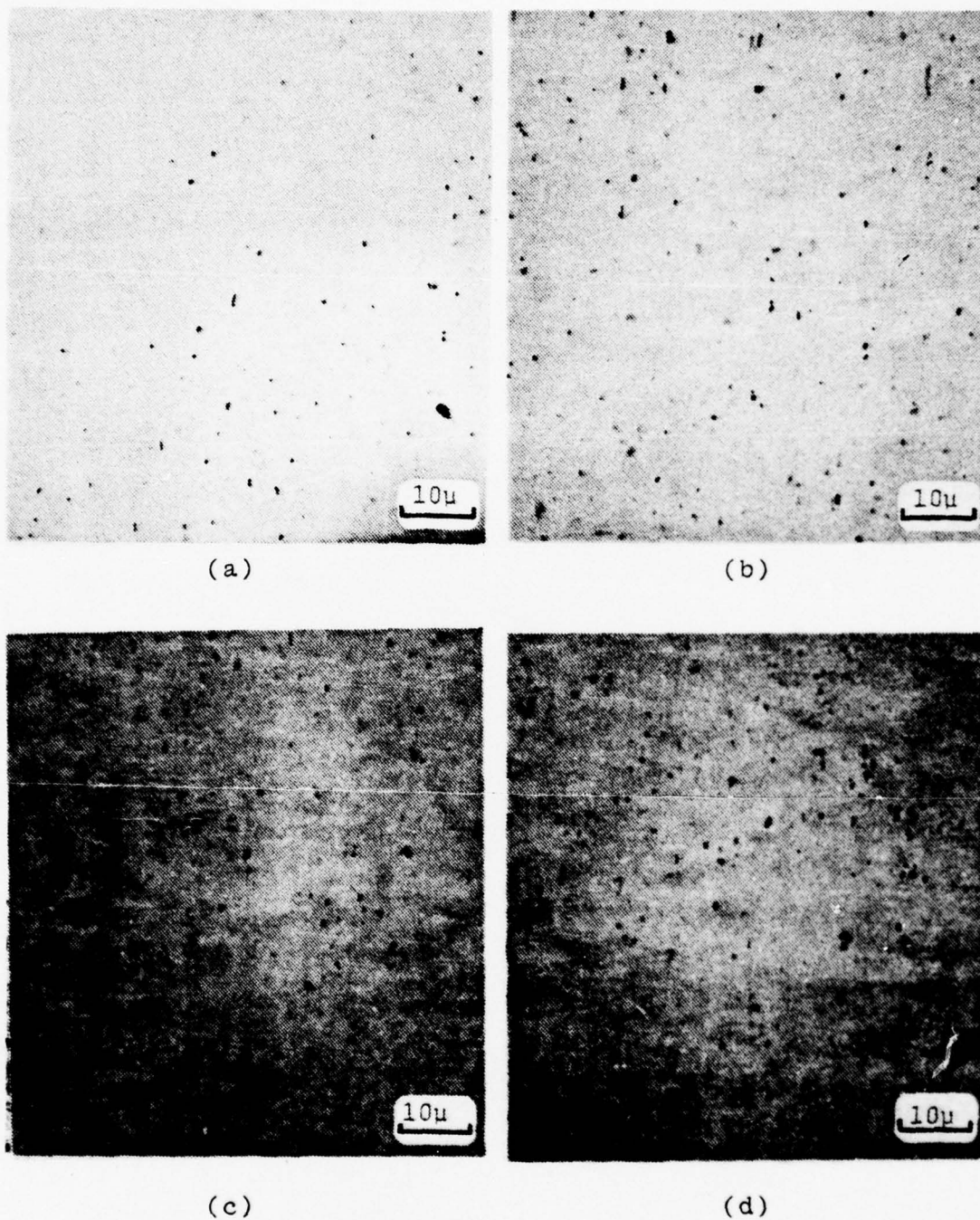


Figure 16. Photomicrographs taken of the "as-polished" specimen subjected to the original two-pass weld only. The locations represented are the interface (a), approximately 6 mm (b), 18 mm (c) and 27 mm (d) from the interface. (100X)

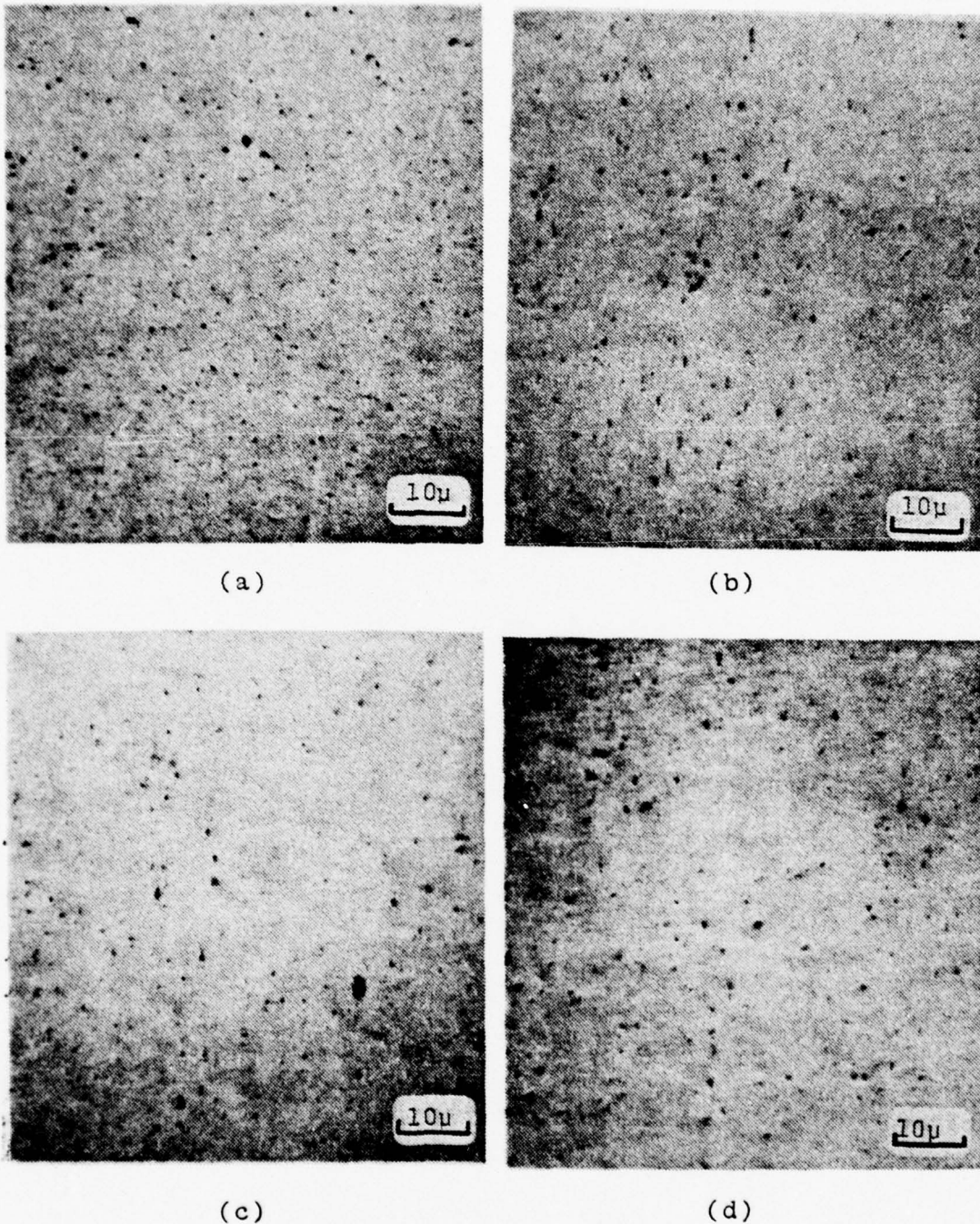
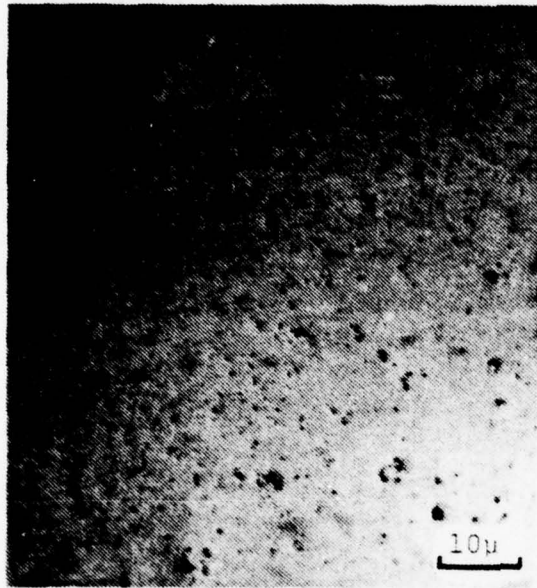
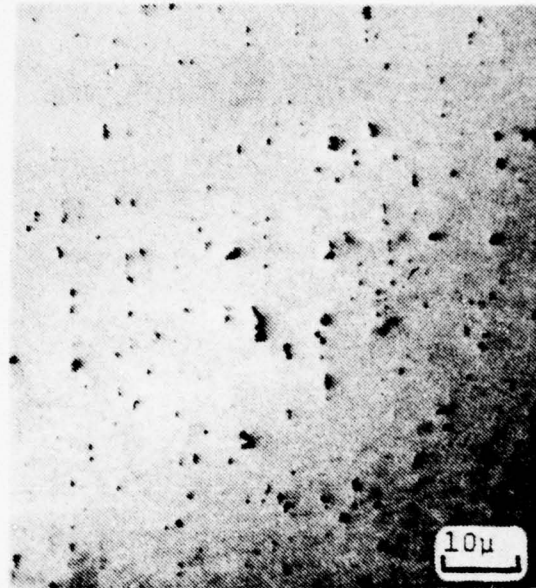


Figure 17. Photomicrographs taken of the "as-polished" specimen subjected to 4 repair simulations. The locations represented are the interface (a), approximately 6 mm (b), 18 mm (c) and 27 mm (d) from the interface. (100X)



(a)



(b)



(c)



(d)

Figure 18. Photomicrographs taken of the "as-polished" specimen subjected to 8 repair simulations. The locations represented are the interface (a), approximately 6 mm (b), 18 mm (c) and 27 mm (d) from the interface. (100X)

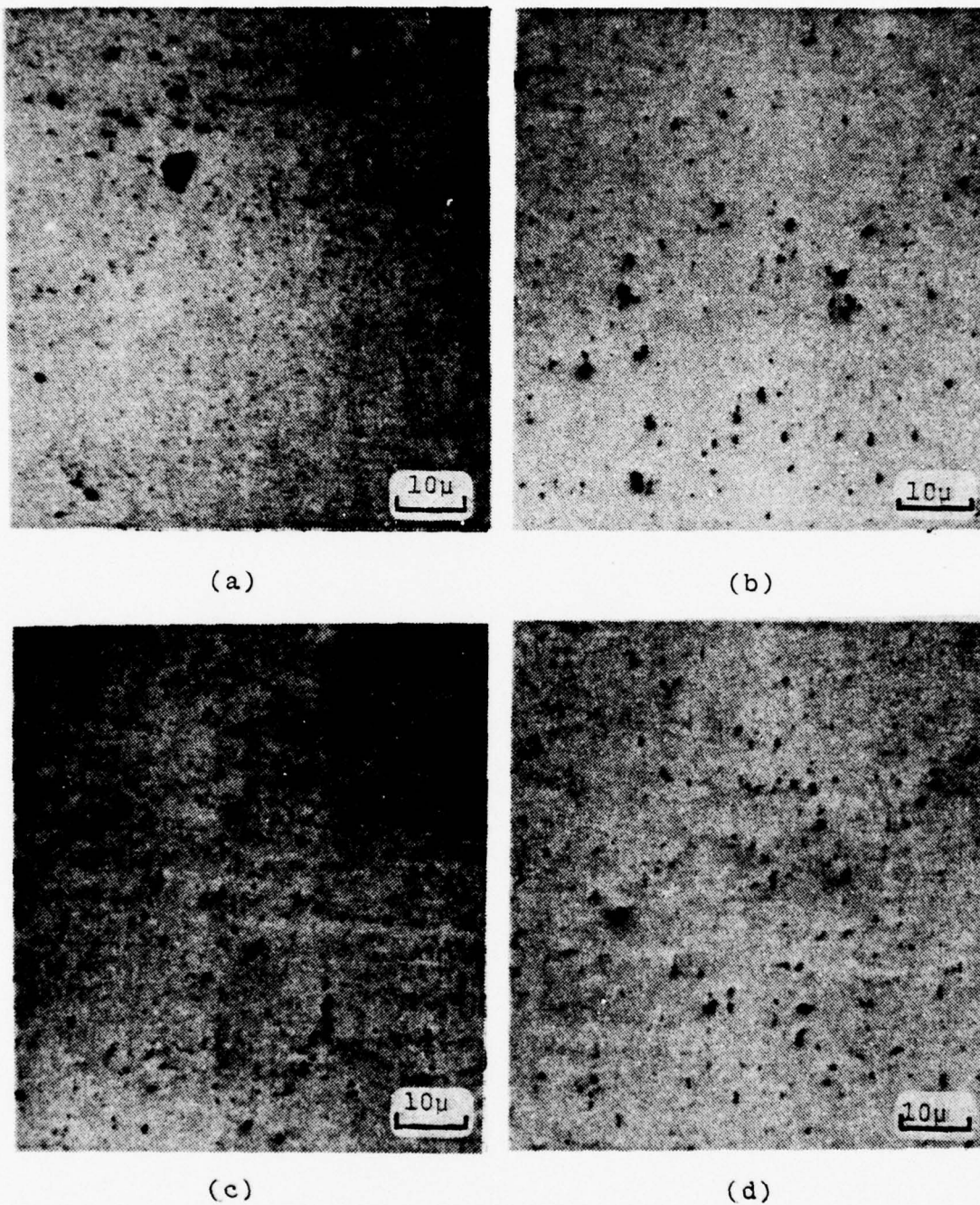


Figure 19. Photomicrographs taken of the "as-polished" specimen subjected to 12 repair simulations. The locations represented are the interface (a), approximately 6 mm (b), 18 mm (c) and 27 mm (d) from the interface. (100X)



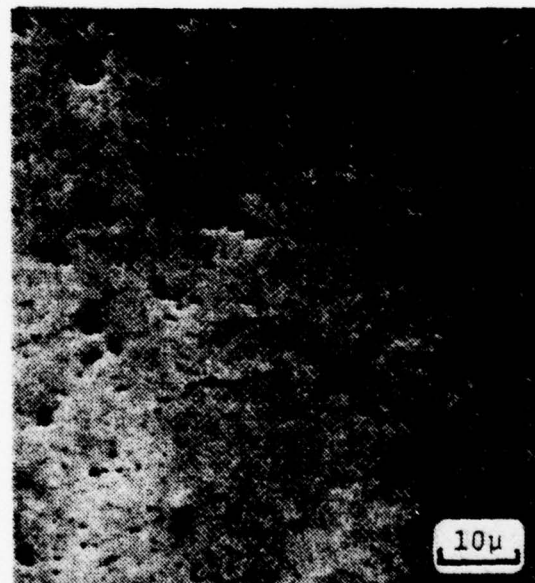
(a)



(b)



(c)



(d)

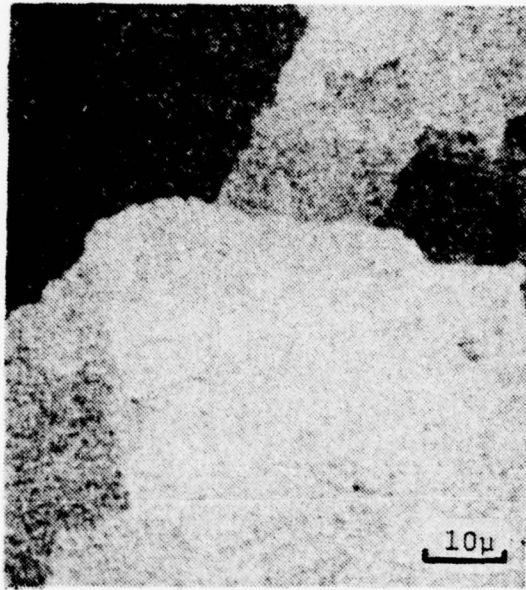
Figure 20. Photographs taken of the "as-polished" specimen subjected to 16 repair simulations. The locations represented are the interface (a), approximately 6 mm (b), 18 mm (c) and 27 mm (d) from the interface. (100X)

micrographs of the specimens taken at locations starting at the interface and at distances of approximately 6, 18 and 27 mm from the interface. Examination of these figures reveals a microstructural change as a function of number of weld repairs. A comparison of these micrographs indicate a distinct coarsening or agglomeration of insoluble precipitates. The degree of coarsening of the precipitate increases with number of weld repairs. The degree of coarsening is most evident in the step from four to eight repairs and from twelve to sixteen repairs. This tendency toward coarsening, although not of a linear progression in a quantitative sense, does show an increase in size and visible numbers with each increase in number of weld repair simulations. It is notable that the precipitate maintained a fairly uniform size and number density from the weld interface throughout the examined length of the individual specimens thus indicating the extent to which such thermal cycling can influence the material (up to a distance of 27 mm from the interface).

2. Microscopic Examination of Grain Size and Morphology In the Etched Condition

Selected photomicrographs of the original two-pass weld, 4, 8, 12 and 16 repair simulations in the etched condition (etchant: modified reagent #12) and at similar locations on each specimen are included in the following pages as Figures 21 through 26.

Figure 21 shows micrographs in the etched condition of the "as-cast" weld metal of specimens subjected to the original



(a)



(b)



(c)

Figure 21. Photomicrographs in the etched condition of the specimens subjected to the original two-pass weld only (a), 8 (b) and 16 (c) repair simulations. The area represented in each of these micrographs is the "as-cast" weld metal. (100X, etchant: modified #12)

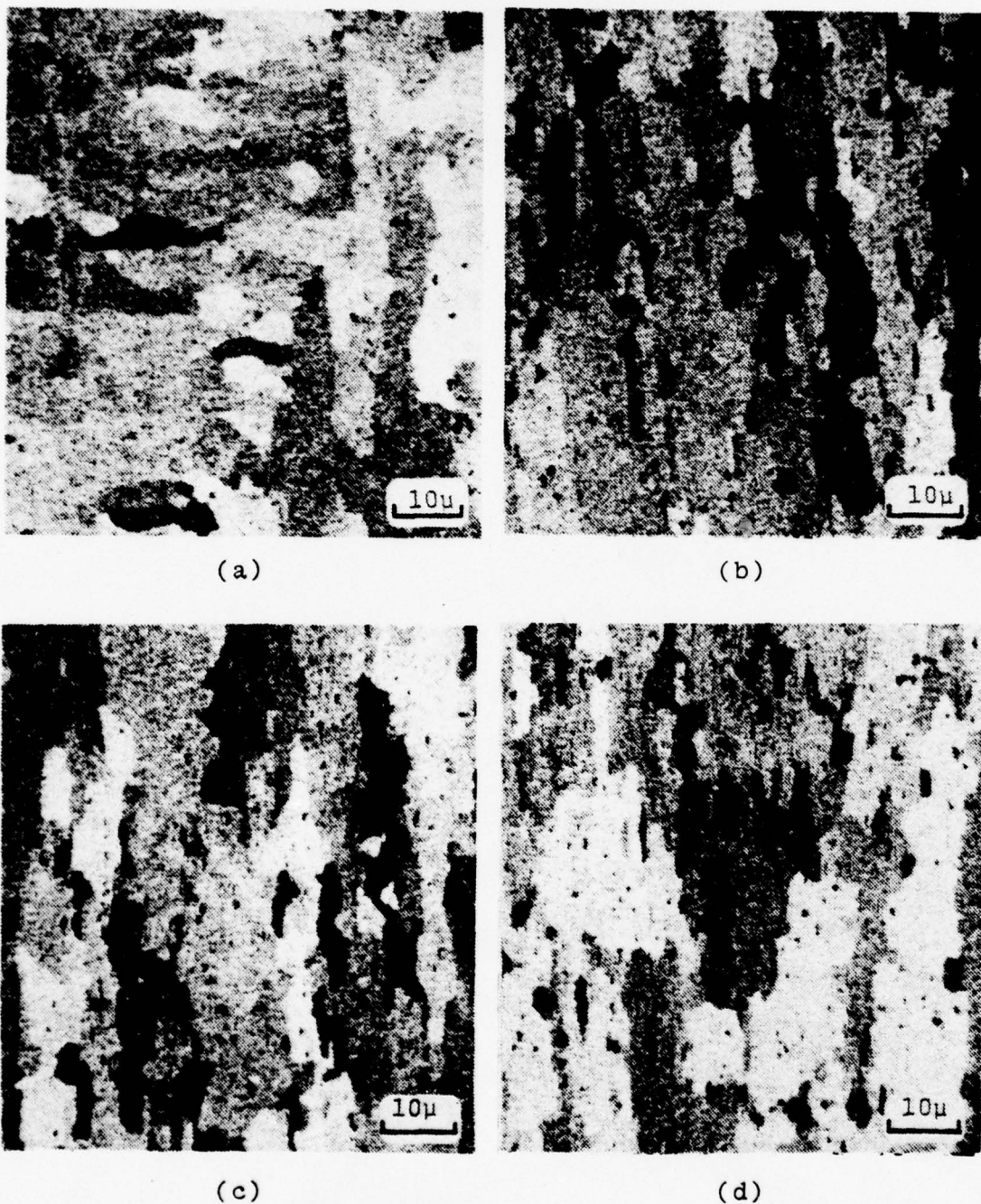


Figure 22. Photomicrographs taken of the etched specimen subjected to the original two-pass weld only. The locations represented are the interface (a), and approximately 6 mm (b), 18 mm (c) and 27 mm (d) from the interface. (100X, etchant: modified #12)

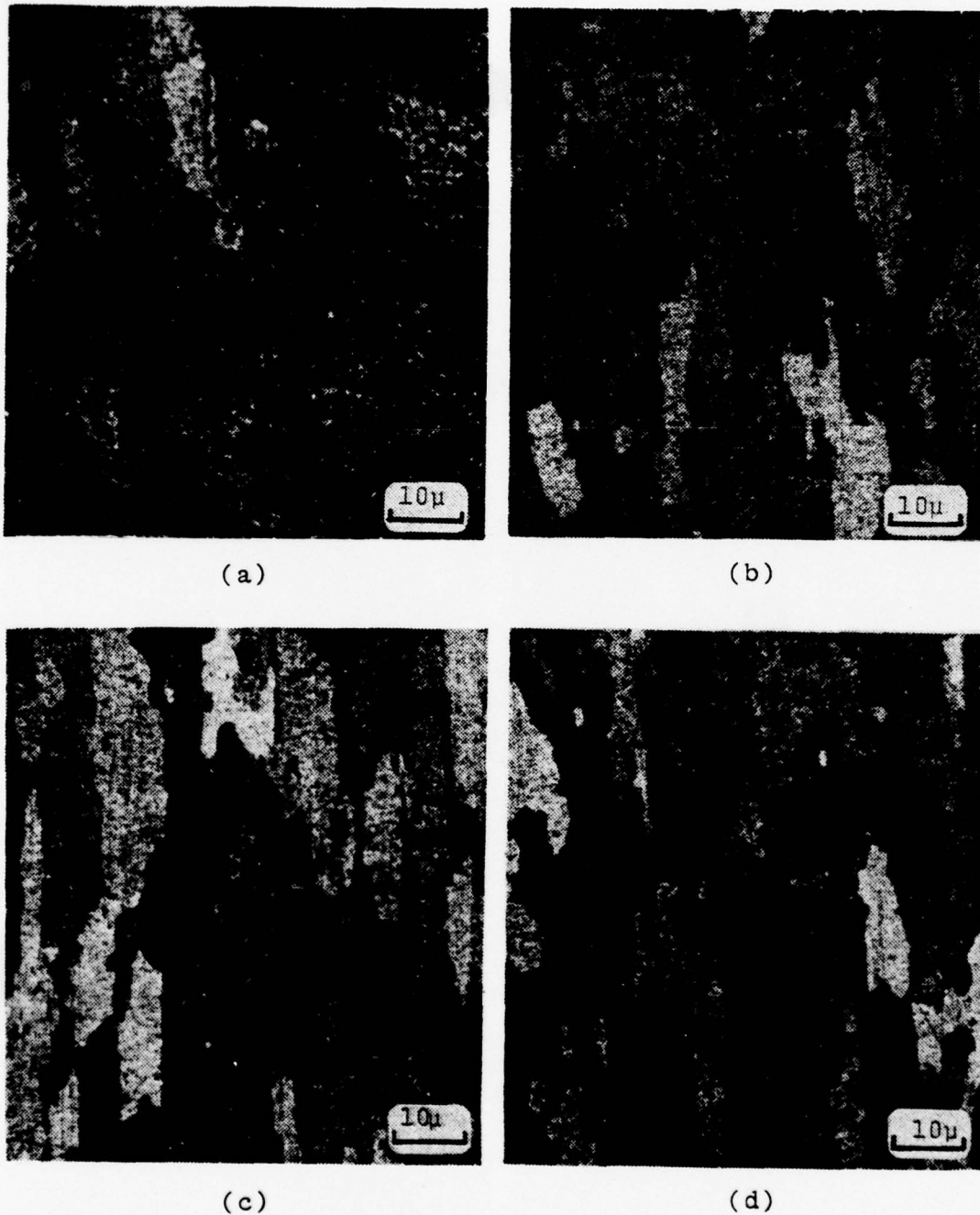
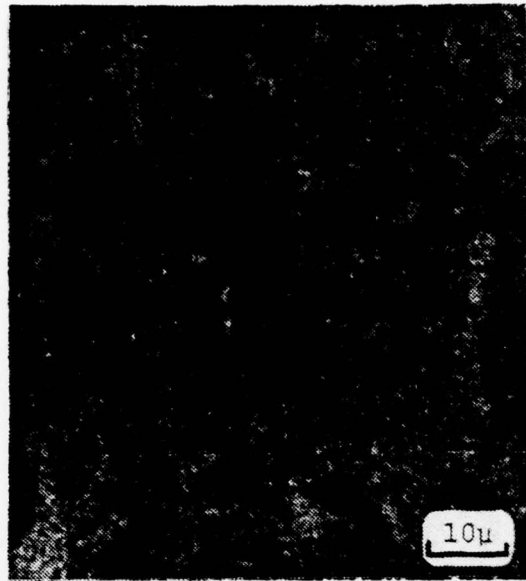


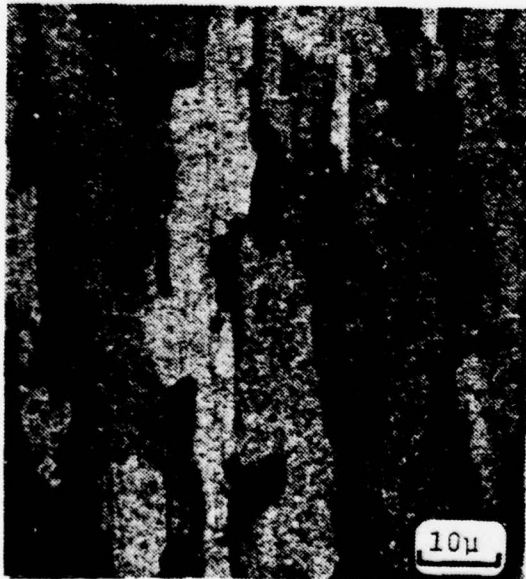
Figure 23. Photomicrographs taken of the etched specimen subjected to 4 repair simulations. The locations represented are the interface (a), and approximately 6 mm (b), 18 mm (c) and 27 mm (d) from the interface. (100X, etchant: modified #12)



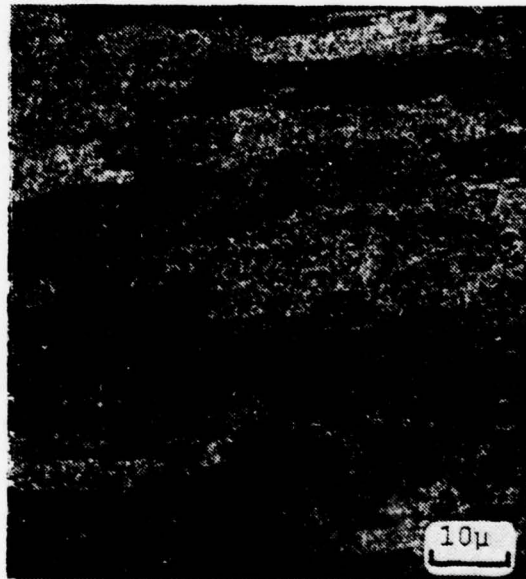
(a)



(b)



(c)

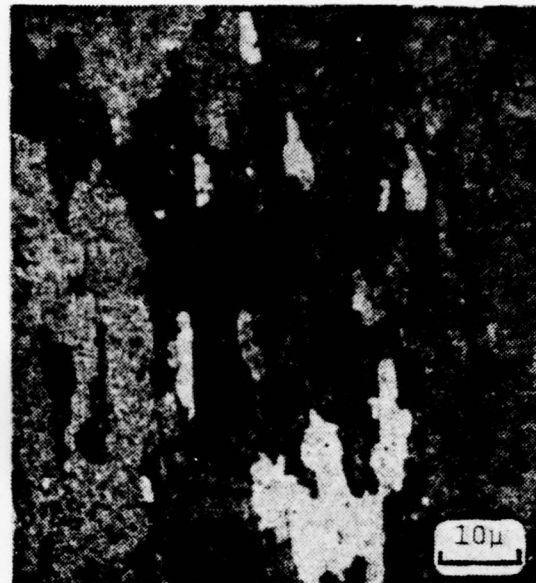


(d)

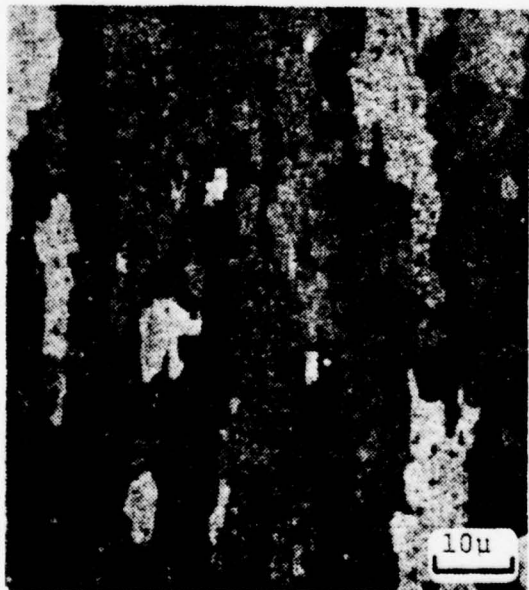
Figure 24. Photomicrographs taken of the etched specimen subjected to 8 repair simulations. The locations represented are the interface (a) and approximately 6 mm (b), 18 mm (c) and 27 mm (d) from the interface. (100X, etchant: modified #12)



(a)



(b)



(c)



(d)

Figure 25. Photomicrographs taken of the etched specimen subjected to 12 repair simulations. The locations represented are the interface (a) and approximately 6 mm (b), 18 mm (c) and 27 mm (d) from the interface. (100X, etchant: modified #12)

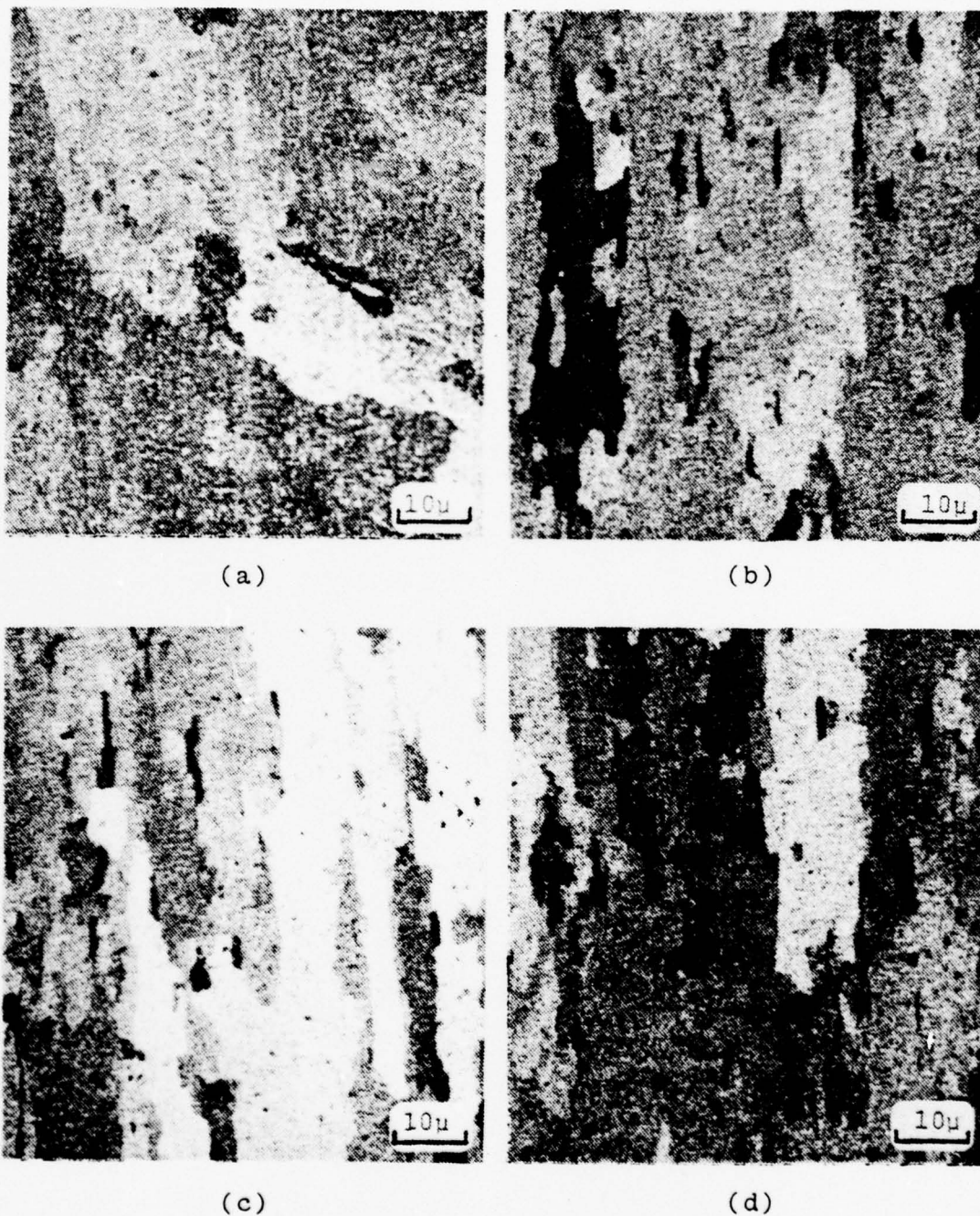


Figure 26. Photomicrographs taken of the etched specimen subjected to 16 repair simulations. The locations represented are the interface (a) and approximately 6 mm (b), 18 mm (c) and 27 mm (d) from the interface. (100X, etchant: modified #12)

weld only, 8 and 16 repair simulations. It is clear from these micrographs that little difference in grain size and shape exists as a function of the number of weld repair simulations. Figures 22 through 26 show micrographs of the specimens in this etched condition taken at locations starting at the interface and at distances of approximately 6, 18 and 27 mm from the interface. A comparison of these micrographs will reveal no significant change in grain size between specimens exposed to different numbers of repairs. This result is expected since the material was in an annealed (and therefore recrystallized) condition prior to welding, any further softening, accompanied by grain size coarsening, as a result of heat input by welding would be slight. There does exist, as may be discerned by comparison of the micrographs, a slight change in grain shape. This change in shape is manifest in a tendency towards more nearly equiaxed grains near the weld interface. The influence of multiple weld repairs on grain size and shape is thus relatively minor. Given the initial annealed condition of the material, it is unlikely that such changes would have any significance relative to the engineering properties of the material.

3. Microscopic Examination Following the Phosphoric Acid Etch

As previously discussed in Section II.D.4., examination following the phosphoric acid etch was performed to investigate the effects of multiple weld repairs upon the preferential

precipitation of insoluble precipitates at grain boundaries. Such an examination was expected to be of use in estimating the material's tendency toward stress-corrosion cracking.

Figures 27 through 29 show photomicrographs of specimens representing the original two-pass weld, and represent an area of approximately 2 mm (0.08 inches) in length, starting with a location in the "as-cast" weld metal approximately 0.5 mm (0.02 inches) from the weld interface. Figure 27 represents that area of the specimen exposed only to the original two-pass weld. Examination of this figure reveals a slight indication of grain boundary precipitation. This is observed as the thin, hair-like lines found in Figure 27 (b) and 27 (c). It should be noted that these precipitate lines are found only in the area beginning at the interface and are concentrated primarily between the interface and at a distance of approximately 0.75 mm (0.03 inches) from the interface. Examination of Figure 28 representing the specimen subjected to eight repair simulations shows an increase in grain boundary precipitation relative to the as-welded specimen. In addition to an increase in numbers of indications, the precipitate lines have become wider and longer. Further examination will reveal that in addition to the definite precipitation lines, very small precipitate particles have begun to agglomerate adjacent to these lines. These fine particles, dispersed about the grain boundaries, are seen to coalesce at the grain boundaries with subsequent repairs as seen in Figure 29. These observations indicate a tendency for the material to exhibit

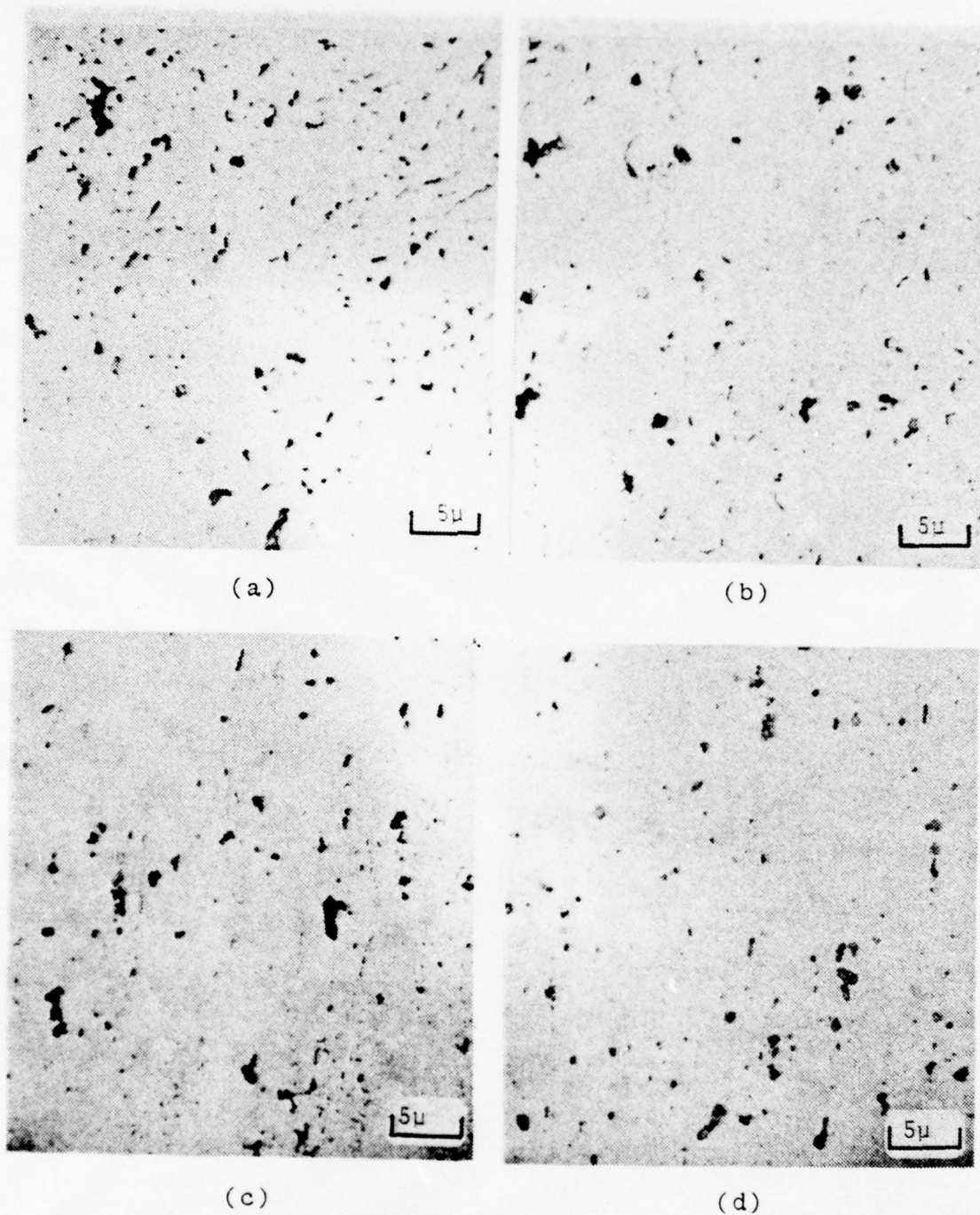
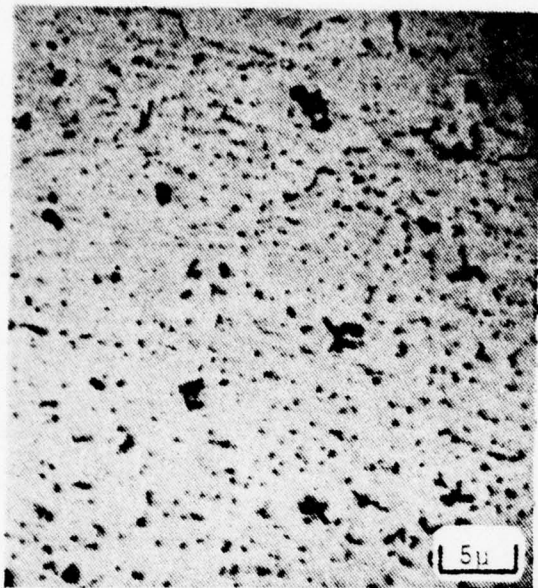
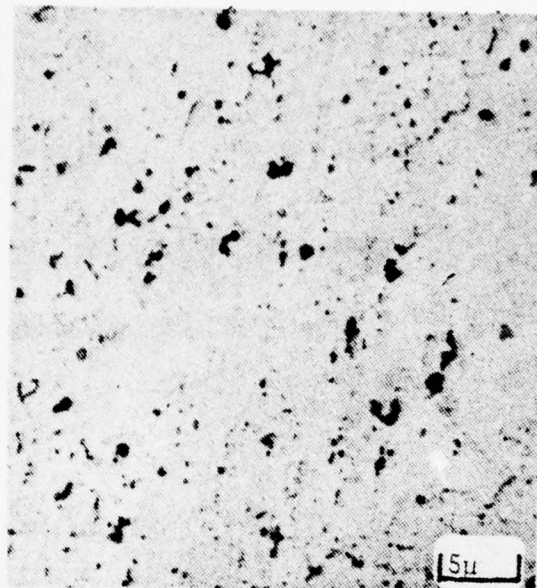


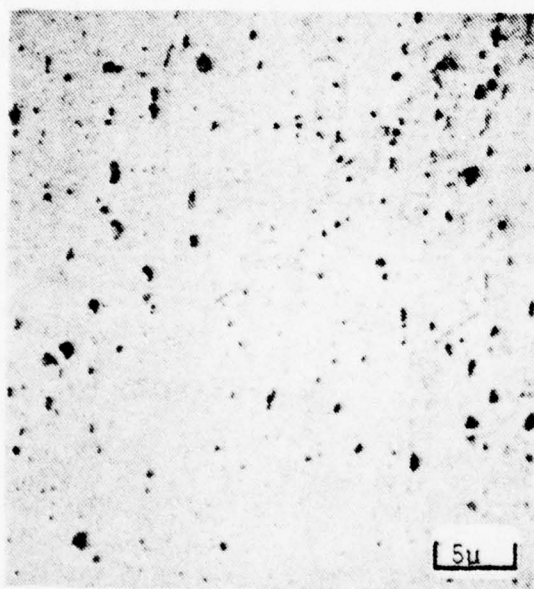
Figure 27. Photomicrographs of the specimen subjected to the original two-pass weld only. These micrographs were taken following etching with the H_3PO_4 solution. (200X, etchant: H_3PO_4)



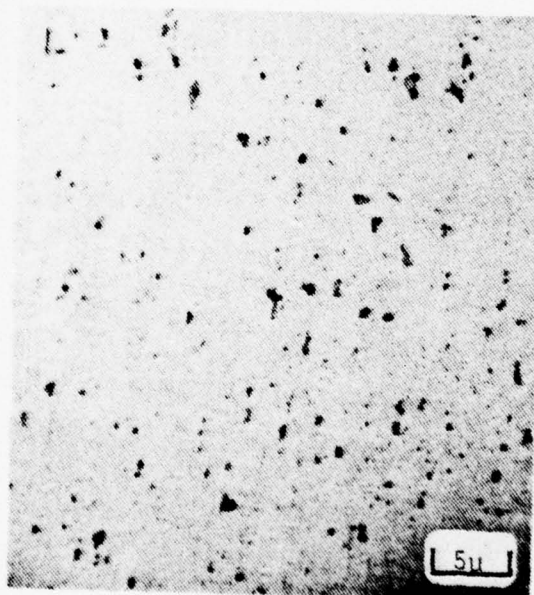
(a)



(b)

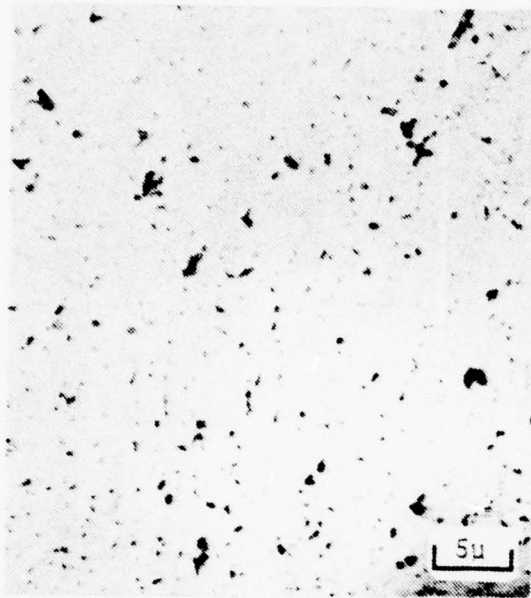


(c)

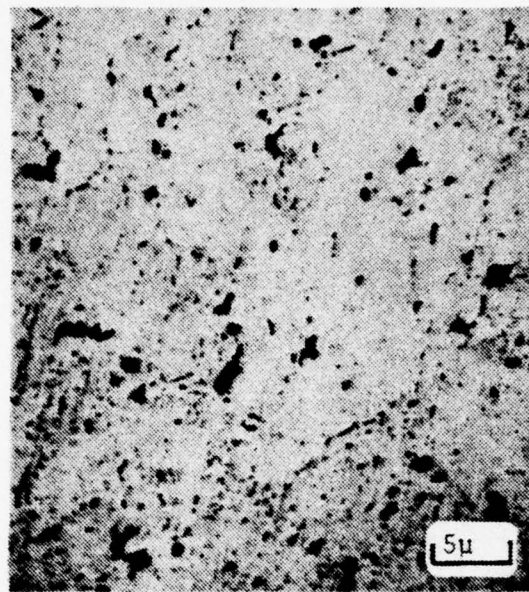


(d)

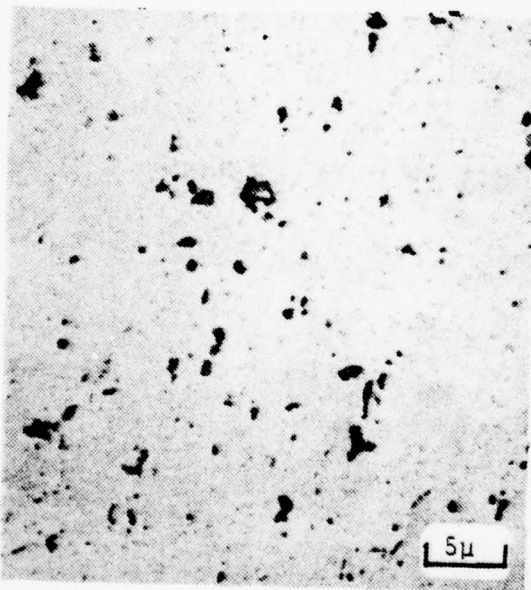
Figure 28. Photomicrographs of the specimen subjected to 8 repair simulations. These micrographs were taken following etching with the H_3PO_4 solution. (200X, etchant: H_3PO_4)



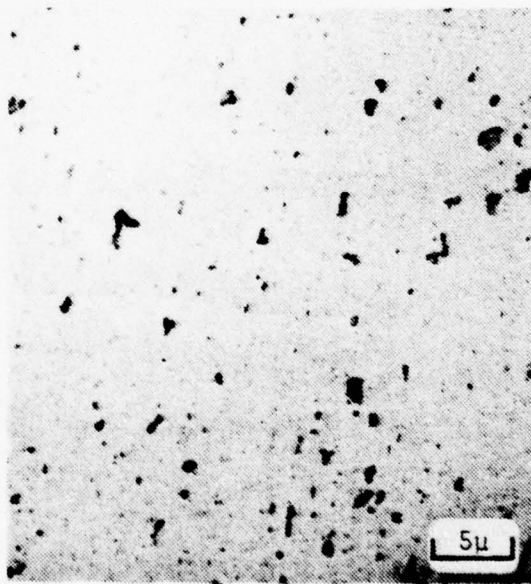
(a)



(b)



(c)



(d)

Figure 29. Photomicrographs of the specimen subjected to 16 repair simulations. These micrographs were taken following etching with the H_3PO_4 solution. (200X, etchant: H_3PO_4)

increased preferential precipitation at the grain boundaries with an increase in number of weld repair simulations. It is also noteworthy that the extent of this kind of precipitation in distance from the interface of the affected area remained essentially constant as a function of increasing number of weld repairs. It is important to note that the formation of the precipitate "necklace" never progressed to the point that it completely encircled a grain.

4. Discussion of the Results of the Microstructural Analysis

Significant observations noted in the metallographic examinations were:

1. the progressive coarsening of the insoluble precipitates as a function of number of weld repair simulations,
2. the lack of change in grain size as a function of number of weld repair simulations,
3. the slight change in grain shape as a function of number of repair simulations, and
4. a slight tendency toward preferential precipitation at grain boundaries as a function of number of weld repairs.

The mechanism for these microstructural changes is, as noted in Chapter I, related to the cycling in temperature between a temperature where the solid solution is thermodynamically stable to lower temperatures where a two-phase material is stable. Finer precipitates will tend to redissolve more readily than coarser precipitates upon heating;

during subsequent cooling, re-precipitation will occur, favoring already existing larger particles (leading to their subsequent coarsening) or in such preferred sites as grain boundaries. Sufficient grain boundary precipitation may result in magnesium-depleted regions near grain boundaries and subsequent sensitization to stress corrosion.

The progressive coarsening of the insoluble precipitates as a function of increased number of repair simulations is not expected to produce any significant change in tensile strength of the material. Because the material was in its softest condition prior to welding, further softening would therefore be slight if at all. For this reason a slight change in grain shape poses no potential problems regarding strength and ductility. The distinct coarsening of the insoluble precipitate could be of significance. Such precipitation could promote a decrease in material ductility by serving as more effective crack initiation sites. Further determination of any degradation in the material's ductility would have to be based on mechanical tests.

The tendency toward preferential precipitation at grain boundaries as a function of number of weld repair simulations also leads to some concern. This mode of precipitation is indicative of increased susceptibility to stress-corrosion cracking. It must be noted, however, that even after sixteen repair simulations the extent of precipitation at grain boundaries remained limited, both to affected area and local extent. The tendency is evident, however, thus suggesting

the necessity to further evaluate the susceptibility of the material to stress corrosion.

B. MECHANICAL TESTING

Mechanical testing was performed to determine hardness, 0.2% offset yield strength, ultimate tensile strength and percent elongation as a function of number of weld repair simulations. Graphical representation of hardness and selected tensile data are shown in Figures 30 through 33. As well, tabulated tensile and elongation data are included as Table II. The results of the mechanical tests are discussed below.

1. Hardness Testing

Hardness testing was performed on specimens from each of the nine test plates. The data were recorded taken along the centerline and at a distance of 3 mm from the centerline of each specimen. The plane of the surface of the hardness specimen is defined by the short and long transverse directions. Thus the lines of the hardness traverses correspond to the midplane of the plate and a plane parallel to the midplane but 3 mm removed. Examination of Figures 30 through 32 reveals that with the exception of a few points, the data fell within a hardness range of from 77 to 83 on the Rockwell F scale. The specimen subjected to the original two-pass weld only exhibited hardness readings taken along the specimen between 78 and 80. These readings indicated no significant

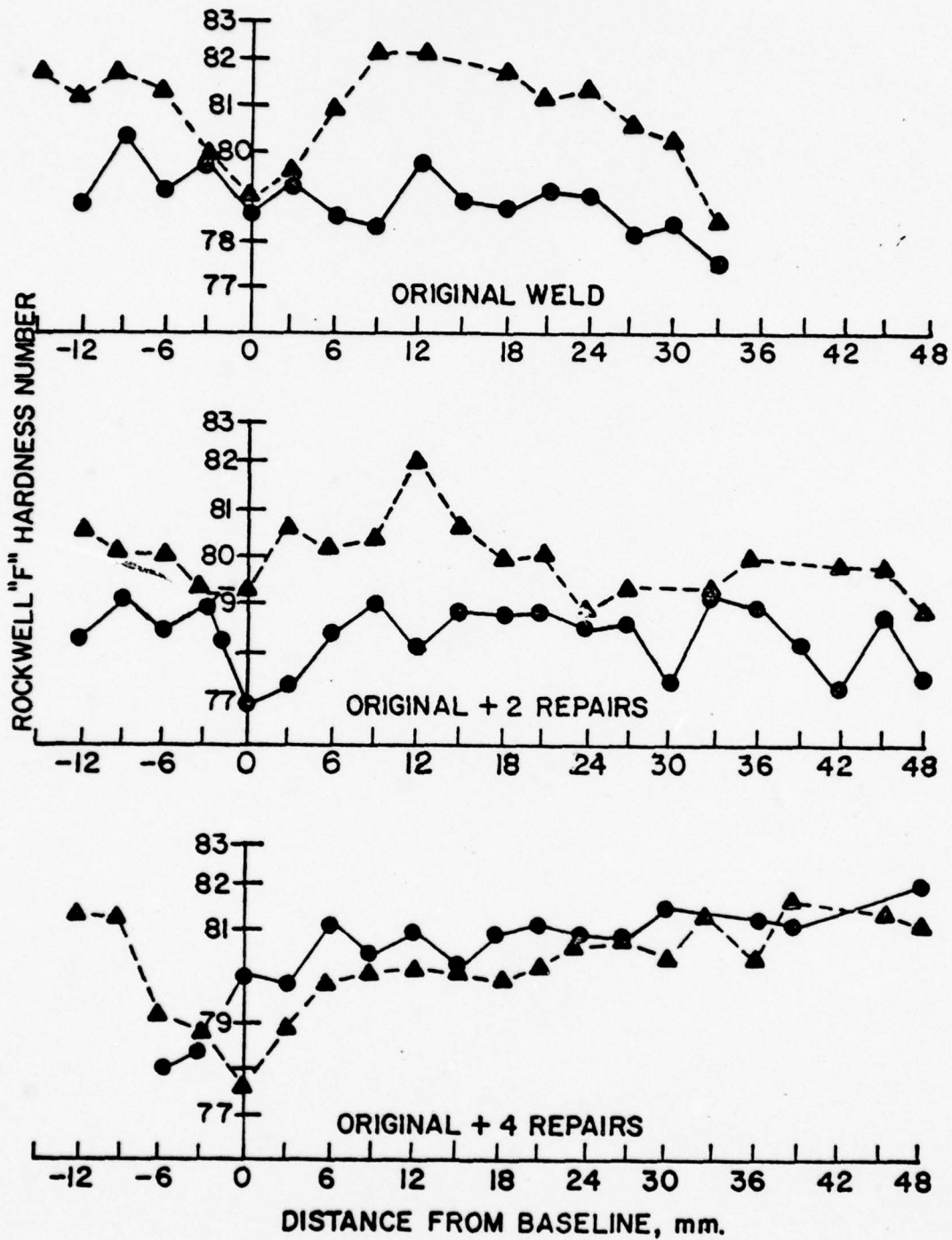


Figure 30. Hardness profiles for specimens subjected to the original two-pass weld, 2 and 4 repair simulations. The solid line indicates data taken along the specimen centerline and the dashed line represents data taken along the line 3 mm from the centerline.

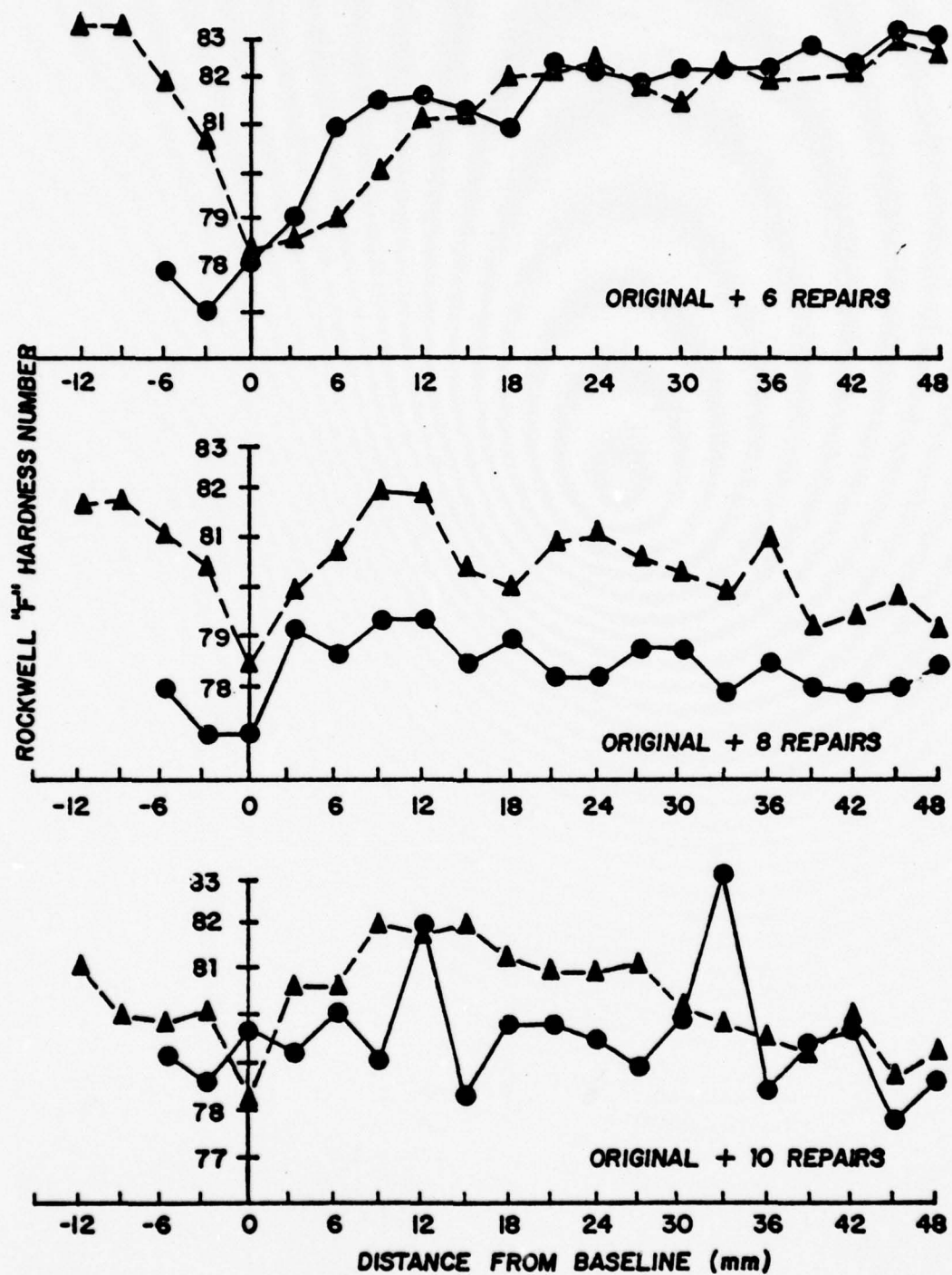


Figure 31. Hardness profiles for specimens subjected to 6, 8 and 10 repair simulations.

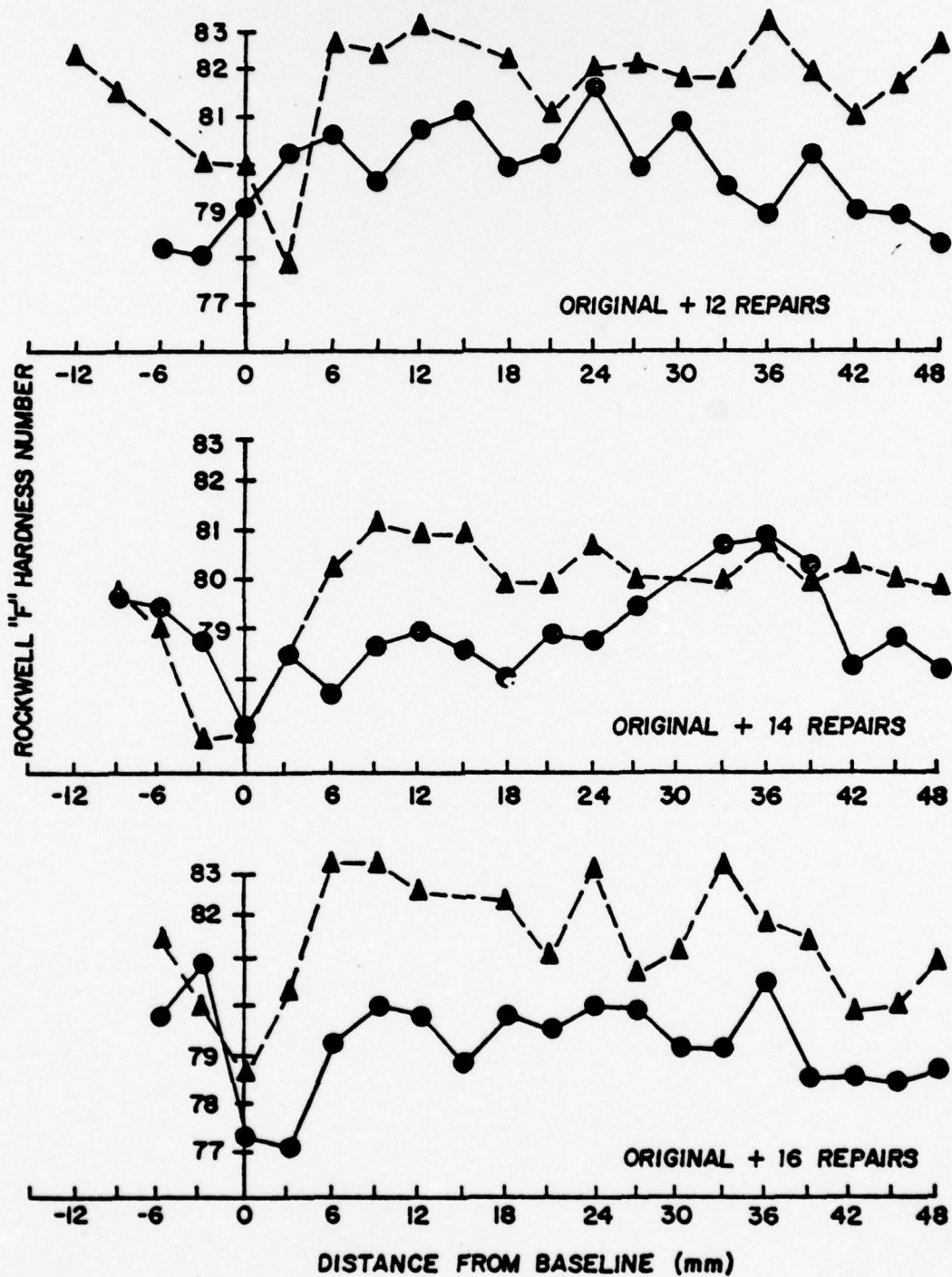


Figure 32. Hardness profiles of specimens subjected to 12, 14 and 16 repair simulations.

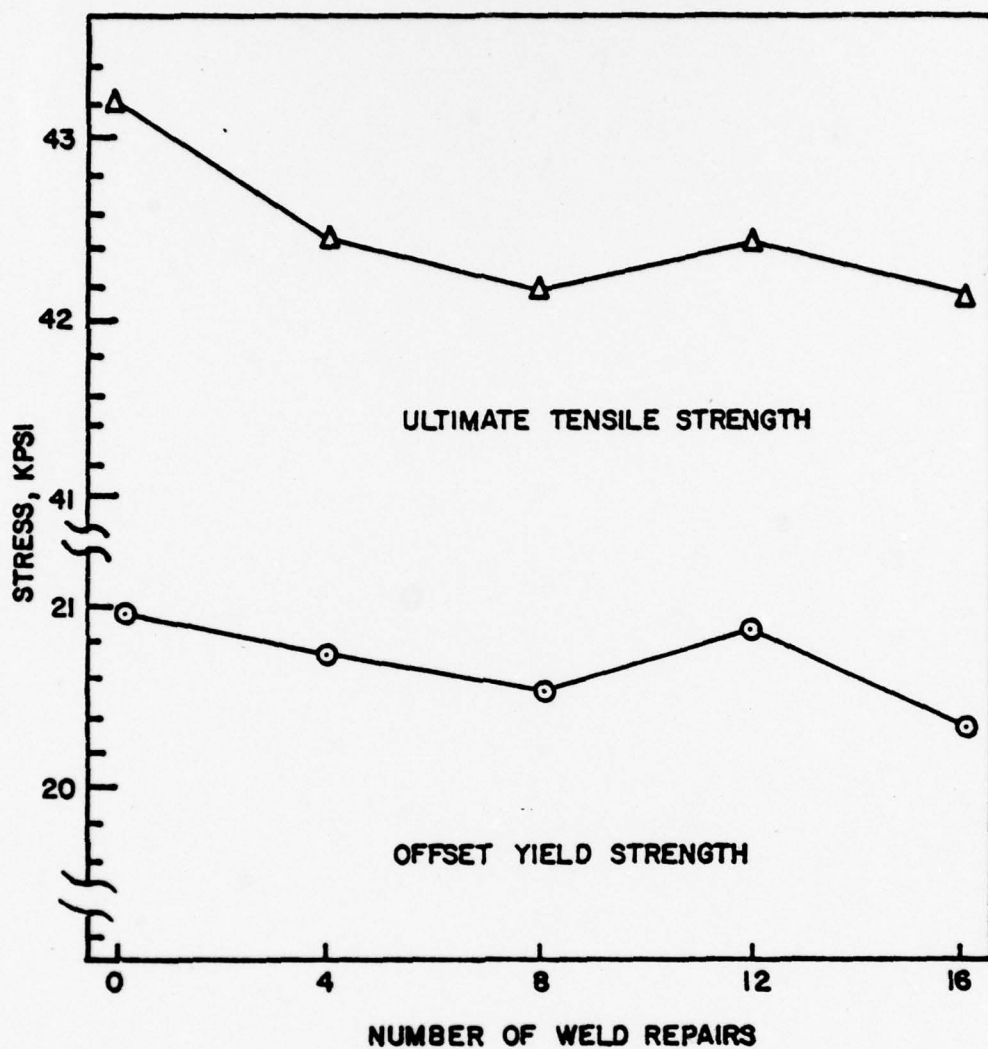


Figure 33. This figure is a plot of the average tensile strengths recorded for specimens subjected to the original two-pass weld only, 4, 8, 12 and 16 repair simulations as a function of number of weld repairs.

TABLE II. TENSION TEST DATA

SPECIMEN #		OFFSET YIELD	U.T.S.	PERCENT ELONGATION
ORIG.	1A	21,120 psi	42,974 psi	17.5
	1B	20,704	43,171	17.5
2 REPAIRS	2A	21,091	42,794	18.0
	2B	21,030	42,918	18.0
4 REPAIRS	3A	21,036	42,702	16.5
	3B	20,353	42,168	16.0
6 REPAIRS	4A	20,704	42,290	16.5
	4B	21,091	42,969	17.0
8 REPAIRS	6A	20,652	42,652	18.5
	6B	20,432	41,558	18.5
10 REPAIRS	7A	18,340	39,655	18.0
	7B	18,473	37,751	18.5
12 REPAIRS	9A	20,394	42,105	19.0
	9B	21,179	42,751	18.0
14 REPAIRS	10A	20,444	41,777	17.0
	10B	20,614	41,447	17.0
16 REPAIRS	11A	20,714	42,142	17.5
	11B	19,742	40,343	18.0

difference in the hardness of the "as-cast" metal relative to the parent plate along the centerline. On the other hand, the data obtained from the same specimen but at a distance of 3 mm (0.12 inches) from the centerline exhibited a rather significant increase in hardness as distance from the baseline increased to a point approximately 8 mm (0.32 inches) from the baseline. The differences in the readings obtained along the two different planes of the same specimen can be attributed to the inhomogeneous deformation during the original rolling of the plate. In general, plate surfaces experience larger deformations during rolling than the interior and are thus more severely strain hardened. Subsequent annealing in this case has not fully homogenized this plate in a mechanical sense. These different locations exhibit slightly different grain sizes, and therefore possible higher hardness values near the surface as a result of greater grain distortion from the rolling process. Examination of the hardness profiles given for each specimen reveal a general tendency for the material to exhibit lower hardness values along the centerline. The only exception to this is the specimen subjected to the four repair simulations. It should also be noted that the data in Figures 30 to 32 are plotted on scales representing a rather narrow range of values of hardness. The error range for such data is typically $\pm 0.5 R_F$, thus explaining much of the apparent scatter between adjacent datum points. This error range results from inhomogeneities in the material as well as the measuring instrument. A progressive comparison

of these hardness profiles does not indicate a well-defined trend as a function of number of weld repairs.

The initial annealed condition of this non-heat treatable alloy precludes any significant changes in hardness due to the heat input during welding. Fixtures used to hold the plates in position during welding do, however, impose mechanical restraint. This restraint, coupled with the thermal expansion and contraction experienced during welding, may lead to some local plastic deformation of the material. The lack of any definite trend in this hardness data suggests, in fact, that the extent of any deformation is minimal, or has been annealed out by the heat input of welding. Thus, it may be concluded that multiple weld repairs have no effect on hardness of the welded plate.

2. Tension Testing

Tension testing was performed on two specimens from each of the nine test plates. This testing was performed to determine offset yield strength, ultimate tensile strength, and percent elongation to fracture as a function of number of weld repairs. Tabulated data for each specimen and a graphical representation of the average tensile strength for specimens representing the original two-pass weld, 4, 8, 12 and 16 repair simulations are included as Table II and Figure 33. The values used in Figure 33 were obtained by averaging the two tensile specimens taken from each test plate.

The commercially required minimum tensile strengths of 5083-0 aluminum in the unwelded condition are 275.8 MPa (40.0 ksi) ultimate tensile strength and 124.10 MPa (18.0 ksi) offset yield strength for material of the thickness used for these tests. The minimum elongation required in a 2-inch gage length is 16%.

The results of the tests, as given in Table II, indicate that the test specimens exhibited mechanical properties above the commercial standards in all but two cases. The two specimens which failed to meet the minimum requirements were 7A and 7B. Both of these specimens were taken from the same test plate. Both of these specimens exhibited ultimate tensile and offset yield strengths less than the minimum required. The cause of this is unknown, however it may be attributable to various causes ranging from surface machining defects to undetermined subsurface inclusions in the weld area. Otherwise, material subjected to both lesser and greater numbers of repairs did meet minimum strength criteria for this alloy. Each of the specimens exhibited final tensile fracture through the weld metal with no crack propagation into the parent plate. Examination of Figure 33 will reveal a slight decreasing trend of the average tensile strengths with increasing numbers of weld repair simulations. This decrease in tensile strength would not have been anticipated considering the fact that all fractures occurred through the "as-cast" weld metal. As mentioned in Section A.1. of this chapter, the "as-cast" weld metal in each specimen should

exhibit duplicate properties. For this reason the effects of multiple weld repairs may not in fact be causing the slight degradation in tensile strength. Since the trend is slight, experimental error must be considered as a possible cause for this observation. In any case this trend is of second order importance in that the strength reduction still leaves the material well within the acceptable performance criteria from an engineering standpoint.

Column 5 of Table II gives elongation data in a two-inch gage length for each specimen. The reader may recall that it was previously suggested in this chapter that there is a possibility of a decrease in specimen ductility as a result of coarsening of the insoluble precipitates with increasing number of weld repairs. Examination of the elongation data obtained, however, reveals that there was no perceptible relationship between material ductility and numbers of weld repairs. This is actually a most gratifying result, particularly in view of the fact that an important property of 5083-0 aluminum considered when designating it for many applications is its ductility.

At the onset of necking elongation ceases to be uniform throughout the length of the specimen. The total extension consists of both the uniform extension up to necking and the localized extension in the necked region. The local extensions experienced in the necked region are larger than those in regions not within the neck [7]. Because of this, an attempt was made to determine how percent elongation was distributed

along the gage length. This was done by placing marks every 0.1 inch between standard 2-inch gage marks. After failure, percent elongation was calculated based on these intermediate marks as well as the standard 2-inch gage length. The results obtained revealed no significant differences in elongation data as a function of multiple weld repairs.

In summary, the results of tension testing revealed no effect on ductility of the specimens as a function of multiple weld repairs and, at best, second order effects on tensile strengths.

C. STRESS-CORROSION TESTS

Section III.A.4. discussed the slight tendency observed toward increased preferential precipitation at grain boundaries with increasing number of weld repairs. Thus, it was felt necessary to further investigate the susceptibility of the welded joint to stress-corrosion cracking as a function of number of weld cycles imposed upon the material. Complications are encountered, however, in the evaluation of different degrees of susceptibility among aluminum specimens which exhibit slight differences in mechanical properties [8]. The question is further complicated by the fact that inhomogeneities exist from specimen to specimen even though they may have been taken from the same plate. Despite these complications, there are several methods for testing 5083 aluminum which have proven reliable and expedient; an in depth discussion of some of these more conclusive test may be found in Refs. [8] and [9].

Because these tests require material, equipment, sensitization and exposure times exceeding the resources afforded this thesis, it was impractical to perform these types of tests. For this reason the tests described in Section II.D.4. were performed using the total immersion method of exposure. Because of the time limitations the results of this test are not considered conclusive at this point and testing will be continued for an undetermined period of time at the Naval Postgraduate School.

Specimens were tested from plates consisting of the original two-pass weld, 4, 8, 12 and 16 repair simulations. As previously discussed, one specimen from each test plate was subjected to an applied stress followed by immersion in pseudo-sea water solution. A second specimen from each plate was sensitized for one week at a temperature of 125°C (257°F), then stressed followed by immersion. The third specimen from each plate was first stressed, then sensitized, followed by immersion.

After a period of 14 days in the pseudo-sea water solution, the specimens were removed and examined for evidence of stress-corrosion cracking. Examination consisted of cleaning the specimens of any deposited salts followed by visual examination utilizing an optical bench metallograph at a magnification of approximately 5 diameters.

This examination revealed a slight corrosive attack in the form of pitting. There was, however, no evidence of stress-corrosion cracking exhibited by any of the specimens. Stressing of the specimens was accomplished by a guided face

bend to a 64 mm (2.5 inch) radius of curvature for the 12.7 mm (0.5 inch) square test pieces followed by loading with a stressing bolt. Thus, the outer face of the weld is subjected to a tensile stress beyond the yield strength, well in excess of any anticipated loading in service. Also, the maximum number of weld repair cycles (16) exceeds the number anticipated in fabrication. The failure to observe any stress-corrosion cracking at this point is therefore gratifying from an engineering standpoint. However, the lack of cracking to date does not indicate whether or not there is a difference in susceptibility as a function of the number of weld repairs. This can only be ascertained under otherwise identical test conditions where cracking would occur in a specimen subjected to multiple repairs and not in a specimen with only the original two-pass weldment (or even in the unwelded plate). For this reason, exposure will continue in order to determine whether or not this is the case. Nevertheless, the result to date does suggest, for engineering purposes, that up to sixteen weld repairs has not induced a gross increase in stress-corrosion cracking susceptibility.

IV. CONCLUSIONS

This investigation has revealed several significant points regarding the effects of multiple weld repairs upon the aluminum-magnesium alloy 5083 in the "O" temper:

1. There has been a definite coarsening of insoluble precipitates as a function of multiple weld repairs. The significance of this coarsening would most likely have been expected to result in a degradation of ductility of the material. Tension testing, however, revealed no tendency for this. It may therefore be concluded that the effects of this coarsening of the precipitates as a function of multiple weld repairs did not affect the ductile properties of this material.

2. There was an observed tendency for the material to exhibit a slight degradation in both offset yield and ultimate tensile strength as a function of increased numbers of repair simulations. For reasons discussed in Section III. B.2., this tendency may in fact not be a function of the increased number of weld repairs but may be attributed to other factors. In any case, the trend toward a decrease in strength was second order in nature and should prove of no great concern to the design engineer.

3. There was an increase in preferential precipitation at the grain boundaries as a function of multiple weld repairs.

This classic indication of increased susceptibility to stress-corrosion leads to some concern.

As discussed in Section III.C., the resultant stress-corrosion tests performed for this thesis did not allow for a conclusive determination as to whether the material would in fact exhibit a greater degree of stress corrosion as a function of numbers of weld repairs. Because of this, the stress-corrosion tests are being continued for an undetermined period of time in an effort to obtain conclusive evidence of the effects of multiple weld repairs upon this materials susceptibility to stress corrosion as a function of numbers of weld repairs. The tests conducted to date, however, did not reveal evidence of stress corrosion in any of the test specimens. Since the degree of stressing, aging (as simulated by the sensitizing procedure) and exposure to a corrosive medium are far in excess to that expected in service for the material used in LNG applications, it may be concluded that the tendency of this material to exhibit a significant degree of stress corrosion under normal service conditions is unlikely.

Further, changes in grain size and shape were proved to be insignificant. Specimen hardness profiles revealed no trends as a function of numbers of repair cycles to which the specimens were subjected.

In conclusion, therefore, it may be stated that this material exhibited no deleterious effects in either a microstructural or mechanical sense as a function of number

of weld repair cycles up to and including the thermal histories represented by the original weld plus 16 repair simulations to which these specimens were subjected.

APPENDIX A. ALLOY CHEMISTRY AND MECHANICAL
PROPERTIES OF 5083-0

Chemical Composition Limits of Wrought Aluminum Alloy 5083

<u>Element</u>	<u>Weight Percent</u>
Silicon	0.40 max.
Iron	0.40 max.
Copper	0.10 max.
Manganese	0.3 - 1.0
Magnesium	4.0 - 4.9
Chromium	0.05- 0.25
Zinc	0.25
Titanium	0.15
Others	
each	0.05 max.
total	0.15
Aluminum	Remainder

Typical Mechanical Properties of Aluminum Alloy 5083-0

Alloy and Temper	5083-0
Strength, ksi (MPa)	
Ultimate Tensile	42(289.6)
Yield	21(144.8)
Elongation Percent in 2 inches	16
Hardness, R_F	79
Ultimate Shear Strength, ksi (MPa)	25(172.4)
Fatigue Endurance Limit, ksi (MPa)	--
Modulus of Elasticity, ksi (MPa)	10.3(71.0)

APPENDIX B

PREPARATION OF PSEUDO-SEA WATER

The following quantities of gravimetric and volumetric salts, combined with enough distilled water for a total weight of 100 kilograms, were used to produce the pseudo-sea water solution for experimentation.

A. Gravimetric Salts

salt	g/kg of solution
NaCl	23.926
Na ₂ SO ₄	4.008
KCl	0.677
NaHCO ₃	0.196
KBr	0.098
H ₃ BO ₃	0.026
NaF	0.003

B. Volumetric Salts

salt	g/kg of solution	ml/kg of solution
MgCl ₂ ·6H ₂ O	1.000	53.27
CaCl ₂ ·2H ₂ O	1.000	10.33
SrCl ₂ ·6H ₂ O	0.100	0.90

LIST OF REFERENCES

1. Young, R. T., The Lessons of the Liberties, American Bureau of Shipping, 1974.
2. Kaiser Aluminum & Chemical Sales Inc., Welding, 1967.
3. Connors, T. G., "Update: Domestic LNG Vessel Construction," Marine Technology, v. 15, Number 1, pp. 1-13, January 1978.
4. Welding Handbook, 7th ed., v. 1, pp.35-99, American Welding Society, 1976.
5. Metals Handbook, 8th ed., v. 8, pp. 120-129, American Society for Metals, 1973.
6. Kester, D. R., Duedall, I. W., Connors, D. N. and Pytkowicz, R. M., "Preparation of Artificial Seawater," Limnology and Oceanography, v. 12, pp. 176-178, December 1967.
7. Dieter, G. E., Mechanical Metallurgy, pp. 342-348, McGraw Hill, 1976.
8. Craig, H. L., Jr. and Romans, H. B., A Rapid Stress Corrosion Test for Aluminum-Magnesium Alloys, Stress Corrosion Testing, ASTM STP 425, American Society for Testing Materials, p. 51, 1967.
9. Brown, B. F., and others, Stress-Corrosion Cracking in High Strength Steels and in Titanium and Aluminum Alloys, p. 147, Naval Research Laboratory, 1972.

INITIAL DISTRIBUTION LIST

	No. Copies
1. Defense Documentation Center Cameron Station Alexandria, VA 22314	2
2. Library, Code 0142 Naval Postgraduate School Monterey, CA 93940	2
3. Department Chairman, Code 69Mx Deaprtment of Mechanical Engineering Naval Postgraduate School Monterey, CA 93940	1
4. Assistant Professor T. R. McNelley, Code 69Mc Department of Mechanical Engineering Naval Postgraduate School Monterey, CA 93940	5
5. LT George R. Speight, Jr., U.S.C.G. Commander (mmt) Eighth Coast Guard District New Orleans, LA 70130	3
6. Mr. Kenneth Graham, Code 61Kg Department of Physics and Chemistry Naval Postgraduate School Monterey, CA 93940	1
7. Commandant (G-PTE-1/72) United States Coast Guard Washington, DC 20590	2
8. CAPT W. D. Markle, U.S.C.G. Commandant (G-M/82) United States Coast Guard Washington, DC 20590	1
9. LCDR Paul Pluta, U.S.C.G. Commandant (G-MMT-2/82) United States Coast Guard Washington, D. C. 20590	1
10. CAPT R. A. Janecek, U. S. C. G. Commandant (G-WLE/73) United States Coast Guard Washington, DC 20590	1